Seismic Imaging and Monitoring with Ambient Noise Correlations

Michel Campillo and Philippe Roux

Institut des Sciences de la Terre, Université Joseph Fourier, CNRS UMR 5275,
Maison des Géosciences, 1381 rue de la Piscine, Campus Universitaire,
38041 Grenoble Cedex 9, France

Table of Contents

1-Introduction

With the development of large networks, huge quantities of continuous recordings have been made available. The extraction of deterministic information about the Earth structure from long ambient-noise time series opens new opportunities for seismologists. Correlations of ambient seismic vibrations are effectively and widely used to reconstruct impulse responses between two passive receivers as if a source was placed at one of them. This provides the opportunity for imaging without a source, or passive imaging. Applications include seismology, helioseismology, underwater acoustics, and structural health monitoring, to cite only a few. This chapter is a brief presentation of the principles leading to the use of seismic ambient-noise correlations as virtual seismograms that correspond to the responses of the Earth between two stations. While the correlation technique went through great development in seismology in the 2000's, the interest in this kind of approach was already stated in earlier studies, such as those of Aki (1957) and Clearbout (1968). Indeed, the same principles have been successfully applied in helioseismology (Duvall et al. 1993). The literature on the subject has grown rapidly, and it would be difficult to include all approaches in this summary. Courtland (2008) related the recent emergence of the method in seismology. Some review papers have already been published (e.g., Campillo 2006, Larose et al. 2006, Gouédard et al. 2008, Wapenaar et al. 2010a, b). The reader can also usefully refer to the book by Sato et al. (2012). This chapter is mostly focused on ambient noise in seismology, while the correlation methods have also undergone important developments with the construction of virtual seismograms from active-source records in exploration (e.g., Rickett and Claerbout 1999, Schuster 2006, Curtis and Halliday 2010, Wapenaar et al. 2010a, b).

In Section 2, we give a brief overview of the nature of the ambient noise in the relevant frequency band for broadband seismometer records. We introduce the correlation method through heuristic approaches in Section 3. Some mathematical results for simple media or simple noise-source distributions are given in Section 4. The limitations of the approach in actual situations are discussed in Section 5. The strategies of processing are presented in Section 6, and examples of applications to imaging and monitoring are presented in Section 7.

2-Noise origin

We recall here some aspects that are important for the applications discussed in the following.

Seismic ambient noise has been studied from the beginning of seismology, largely because of the need to improve the level of detection of deterministic arrivals. From early studies (e.g., Gutenberg 1958), it was recognized that the origin of the permanent agitation of the ground surface is different for different frequency bands. The high frequency noise (f >1 Hz) is generally due to human activity (e.g., machinery, traffic). The energy of these signals is strongly variable in time, and is correlated with human life rhythms, with day and week periodicities. On the contrary, the natural origin of long-period ambient noise was recognized through the correlation of the amplitude with meteorological conditions. The frequency limiting the domain of human activity is dependent on local conditions (e.g., Bonnefoy-Claudet et al. 2004). As no generalities can be drawn for high frequency noise, we will concentrate our discussion in a low frequency band that is well defined globally as associated with the interaction of the oceanic swell with the solid Earth. In the band of 0.3 Hz to 0.05 Hz, the ambient noise is often referred to as 'microseisms'. Note that the general issues discussed in the following for the correlation of microseism records also apply for anthropic noise at high frequency. Microseisms have large amplitudes that provide an obstacle for the detection of weak arrivals produced by earthquakes. As the detectability level is an important issue in seismology, microseisms have been extensively studied. In the microseism spectral band, the noise is dominated by surface waves, which are predominantly Rayleigh waves (e.g., Toksoz and Lacoss 1968). The presence of body waves has nevertheless been attested (e.g., Vinnik 1973). The coincidence between periods of strong microseisms and high swells that reach the coast-line was noted early on (Gutenberg 1924). Toksoz and Lacoss (1968) used array analysis to demonstrate the correlation between microseism sources and regions of low atmospheric pressure.

Two peaks dominate the spectrum of microseisms, the principal one being for a period between 5 s and 7 s, while a less marked peak is also observed at twice the period of the main peak (e.g., Peterson 1993). These general characteristics are interpreted as the footprint of the spectrum of oceanic gravity waves.

The less energetic, single-frequency or primary microseisms peak, at periods around 14 s, is similar to the spectrum of wind-generated ocean gravity waves (Haubrich et al. 1963). With the limited penetration of gravity waves at this period, the noise is expected to be produced in shallow waters, and to be amplified by shoaling. To decipher the geographical origin of the primary microseism, Stehly et al. (2006) analyzed the energy of long-term average noise cross-correlations as a function of the azimuth of the station direction. The distribution of sources shares great similarity with the map of average ocean wave heights

obtained from satellite observations, which shows zones of primary microseism excitation in oceanic deep basins, with a seasonality of the global contributions from northern and southern oceans.

The stronger double-frequency, or secondary microseism, peak at a period around 7 s is interpreted as the result of nonlinear interactions between ocean gravity waves propagating in opposite directions, as shown by Longuet-Higgins (1950) based on earlier studies of Miche (1944). This nonlinear process produces a pressure at the sea bottom, even when the height of the water column is greater than the gravity-wave wavelength. The amplitude of the excitation depends on the response of the resonant water layer for specific periods and bathymetry. The microseism excitation depends on the ocean-wave state (swell amplitude), the existence of wave trains in opposite directions, and the bathymetry (resonance condition). The existence of gravity waves that propagate in opposite directions can be due either to reflection along the coast or to specific conditions of storm systems in the deep oceanic basins (e.g., Kedar et al 2008, Zhang et al. 2010). Teleseismic body waves are identified using beam forming, by their high apparent velocity, and they have been used to map the actual sources in the oceans (e.g., Landès et al. 2010). Recent analyses have suggested that both coastal and deep-water origins are represented in the actual observations (Ardhuin et al. 2011, Hillers et al. 2012), and it has been demonstrated that global oceanographic models of sea state coupled with the physical description of the excitation allows for independent prediction of the main patterns of secondary microseism sources.

At long periods, i.e., below 50 s, the ambient noise that is often referred to as hum has the spectral structure of the free oscillations of the Earth (e.g., Kobayashi and Nishida 1998, Tanimoto et al. 1998). The origin of this excitation is assumed to be the interaction of the ocean infragravity waves with the solid Earth. This mechanism was confirmed by the correlation between the apparent locations of hum sources with regions of large wave heights (e.g., Rhie and Romanowicz 2004). Nishida et al. (2008b) showed that the generation of background ambient noise at long periods occurs both in coastal regions and in deep oceans. The normal pressure caused by oceanic waves on the sea bottom can account for spheroidal motions. However, large toroidal contributions (e.g., Kurrle and Widmer-Schnidrig 2008) and long-period Love waves (Nishida et al. 2008) have been observed. This was explained by Fukao et al. (2010), who proposed a model for the coupling of infragravity waves with the topography of the sea bottom.

In conclusion of this short presentation, it appears that the origin of the seismic ambient noise is still the object of on-going research and discussion. Different processes are

invoked exclusively for the two main spectral peaks and the long period domain in spite of the continuous character of the noise spectrum.

3-Principle of the method: the heuristic approach

In this section we present simple physical views of the principle of the ambient-noise correlation method. The mathematical developments are discussed in the next section.

The results presented here originate from previous studies in seismology that were aimed at using ambient noise to extract deterministic information relating to the Earth structure (e.g., Aki 1957, Clearbout 1968). In seismic exploration, the 'daylight imaging' method was pioneered by Claerbout (1968), who proposed the conjecture stating that the cross-correlation of two daylight traces at surface locations A and B is equivalent to a reflection trace at B generated by a source at A. A formal demonstration was given for the one-dimensional (1D) case. The same idea was then successfully applied in time-distance helioseismology (e.g., Duvall et al. 1993).

The correlation function of the fields recorded at two points is used as a virtual seismogram for which the source is acting at one point and the receiver at the second. For two signals of duration T, the correlation of the signal $u_1(t)$ at $\vec{r}_1$ and $u_2(t)$ at $\vec{r}_2$ is defined classically in the time domain as:

$$C(\vec{r}_1,\vec{r}_2;t) = C_{1,2}(t) = \frac{1}{T}\int_0^T u_1(\tau)u_2(t+\tau)\,d\tau \qquad (1),$$

or equivalently in the frequency domain as:

$$C(\vec{r}_1,\vec{r}_2;\omega) = C_{1,2}(\omega) = u_1(\omega)u_2^{*}(\omega) \qquad (2).$$

The correlation function is widely used to measure the resemblance of two signals, and when these signals are similar enough, the time delay that separates them. The ambient noise signals recorded at distant stations are considered to be uncorrelated, as these result from variable interference between numerous waves of different types emitted by different sources. The same argument holds for the scattered waves that comprise the coda of seismograms.

Noise-correlation methods aim at extracting the slight coherent part of the signals that contains deterministic information on wave propagation between the two stations. Indeed, in a medium governed by a wave equation, the motion at two points cannot be fully independent. The extraction of the wave response between the two points is made possible by averaging the correlation over the positions of the sources of the signals. Note that, in the reasoning, the sources include the scatterers viewed as secondary sources.

3.1-The time-reversal approach

A simple, heuristic approach is based on the analogy between a correlation and a time reversal experiment (e.g., Derode et al. 2003, Paul et al. 2005). While not completely rigorous in a general case, this analogy allows for an understanding of the physical processes behind the noise-correlation method. In a time-reversal experiment in the laboratory, signals from an active source are recorded, numerically reversed ($t \rightarrow -t$), and then re-emitted in the medium (e.g., Fink 1992). According to the time symmetry of the solutions of the wave equations, the waves propagate, and under certain conditions, they focus on the original source position. In a scalar case, the conditions in such an experiment are that the recording–re-emission point distribution is sufficient to reconstruct the angular range of the original wave field. Typically, this is the case with a closed cavity that contains the source. When the re-emitted field is perfectly focused, the focal point can be considered as a virtual source. In seismology, we have no device that can emit a complex signal with sufficient energy. Our approach to the construction of signals from virtual sources is completely passive. We consider the mathematical analogy between correlation and convolution by a time-reversed signal. Indeed, the cross correlation of the signal produced by a source in S at receivers at A and B is formally equivalent to having a source at A producing waves that are recorded at S, time-reversed, and re-emitted from S, to be recorded at B (as written in the frequency domain in Equation (2)).

We have illustrated these operations in Figure 1 with numerical simulations. For the sake of simplicity, we consider 2D scalar propagation in a weakly scattering medium (Paul et al. 2005).

Figure 1. *Numerical simulation of the reconstruction of the causal and anti-causal parts of the Green's function from cross-correlations. (a) Configuration of the numerical experiment. One thousand sources S (x) surround the reference point A (+). Dots indicate the point scatterers. (b) Snapshot of the cross-correlation between the field at A and the field at*

location (x, y), after averaging over the sources S for the correlation time of 30 s. The weakly diffusive medium is characterized by the transport mean free path l = 640 km, which is greater than the distance between the points where the correlations are computed. A converging wave front is well defined and constitutes the anti-causal part of the Green's function. (c) Snapshot for correlation time t = 0 s. The wave front is focused on A. (d) Snapshot for t = 30 s. The diverging wave front corresponds to the causal part of the Green's function (a to d are from Paul et al. 2005). (e) Snapshots of the actual noise correlation computed from a network in western USA showing the causal surface wave part of the Green's function (from Lin et al. 2009).*

The field produced by each of several sources S along a circle is computed at each point of the medium (Figure 1a). The signals are cross-correlated with the signal of a central reference point. The correlations are shown in Figure 1b-d for correlation times -30 s, 0 s and 30 s. At time $t = 0$, all of the energy is focused on A, as if A was a source. We observe a converging wave front for negative correlation times, and a diverging wave front for positive correlation times. These wave fronts correspond to the causal (positive times) and anti-causal (negative time) parts of the Green's function between A and any point R in the medium. The nearly perfect reconstruction of the Green's function, similar to a perfect time-reversal mirror, is explained but the perfect distribution of the source around A and R. To illustrate a practical application, snapshots of ambient noise correlations produced with USArray data (Lin et al. 2009) are presented in Figure 1e. The clear diverging surface wave front suggests that the array is surrounded by distant noise sources.

3.2-Stationary phase and end-fire lobes

Following the time-reversal analogy, it can be asked whether the noise sources that surround the two receivers in the correlation process all contribute in the same manner to the reconstruction of the Green's function. In the absence of scatterers that can redirect the field in all directions, the Green's function emerges from the correlations that contain noise sources where their acoustic path passes through one receiver to reach the other one.

An experimental demonstration of this process was performed from ocean data simultaneously recorded on two sono-buoys at a few hundred meters from each other in a shallow-water environment. Noise was generated over 16 min in the 100 Hz to 300 Hz frequency interval using a ship, the track of which is represented in Figure 2a. The two 16-min-long time-series are then cross-correlated using different time windows (Figure 2b-f).

When the correlation is performed on 1-s-duration time series (Figure 2b), the ship track is clearly observed. If the length of the cross-correlated time series is increased to 5 s, 10 s, 20 s and up to 30 s (Figure 2b-e, respectively), the signature of the ship track tends to disappear and the only signal left is obtained when the ship crosses the end-fire main lobes, which is defined as the directivity pattern of the time-domain cross-correlation between the two sensors (Figure 2a).

Figure 2. *(a) Representation in latitude-longitude coordinates of a 16-min-long ship track (blue full line) with respect to the sono-buoy locations (blue '*'). The approximate distance between the sono-buoys is R, at ca. 650m. The average ship speed was constant, at 4.8 m/s. The labels along the ship track correspond to each minute of the recording time window. The end-fire directivity pattern of the two sono-buoys is plotted in red. (b-f) Representations of the temporal evolution of the time-domain cross-correlation function between the two sono-buoys along the 16-min-long ship track. The x-axis and y-axis correspond to the time axis of the correlation function and the recording time, respectively. The duration of the time windows on which the cross-correlation was performed was (b) 1 s, (c) 5 s, (d) 10 s, (e) 20 s, and (f) 40 s. Each cross-correlation pattern is normalized relative to its maximum. The color scales are in dB (from Roux et al. 2004).*

When coming from the end-fire lobe of the two receivers, the signal is produced by a noise source where its acoustic path that passes through one receiver naturally reaches the other receiver. The signals are then similar at the two receivers and contribute coherently to the correlation process with a unique delay time that corresponds to the travel time between the receivers. On the contrary, for a noise source outside the end-fire lobe, the ray paths that connect the source to each receiver do not superimpose. The sources out of the end-fire lobes do not contribute coherently to the correlation, as the correlated waveforms correspond to time delays that vary rapidly with the noise-source position.

Obviously, we observe in Figure 2b-f that the longer the correlation window, the higher the signal-to-noise ratio (SNR), because more acoustic sources participate coherently to the correlation function when the incoherent contribution averages out. Indeed, assuming that the speed of the ship was constant during the track, it generates a uniform density of sources over time. For long time windows, the SNR of the correlation process can be defined as the ratio of the number of coherent *versus* incoherent sources inside the recording time window.

In summary, the averaging of the correlation process over time magnifies the coherent *versus* incoherent contributions of the noise sources. Following the geometrical interpretation, the coherent *versus* incoherent ratio corresponds to the area enclosed by the end-fire beam to a non end-fire beam.

Finally, note that the time-averaged correlation function in Figure 2f shows different bottom-reflection and surface-reflected paths that correspond to the arrival-time structure of the Green's function in a shallow-water environment.

Figure 3. *(a) Experimental geometry when considering sources that surround a receiver-pair. The selection was for 240 sources located between two circles of radius R1 = 300 m and R2 = 370 m, which were centered at the middle of the receiver pair. (b) Average intensity of the raw traces with definition of the time windows corresponding to direct arrivals and to coda. (c) Cross-correlation functions obtained from each source and plotted as a function of azimuth θ (see definition on the insert). (d) Actual experimental Green's function and cross-correlation averaged over the sources (see panel (a)). (From Gouedard et al. 2008).*

Another way to understand the Green's function reconstruction is to separate the contribution that each noise source has to the correlation process. This was made possible with actual data from a high-resolution survey performed by Petroleum Development Oman (PDO) in North Oman. During this active-seismic survey, a large set of 1600 vibrators were used in combination with 1600 receivers over a 1-km square area, to measure the 1600 × 1600 time-domain signals that constituted an exhaustive measurement of the transfer function of the half-space medium.

From this dataset, we select a pair of receivers that are separated by a distance of d = 158 m, with a midpoint that coincides with the center of the ring in Figure 3a. This ensures the same scattering regime for both of the receivers at a given time of the records. Integrating over a line surrounding the receiver pair is theoretically sufficient to get the Green's function, as in our case the medium is lossless. As shown in Figure 3a, we selected sources inside a ring to increase the SNR when computing the cross-correlation. We define the azimuth with respect to the receiver pair, denoted by θ, as the difference between the azimuth defined by one source and the receiver pair center and the receiver pair azimuth (Figure 3c, insert).

The end-fire lobes of the receiver pairs are the areas located in the alignment of the receivers (one on each side). The end-fire lobe aperture depends on the ratio between the

wavelength and the range between the receivers (Roux and Kuperman 2004), and corresponds to the misalignment of the source with respect to the receiver pair. Sources exclusively located within the end-fire lobes induce time delays between the apparent travel time at the two receivers that are smaller than 1/8 of the central period associated to the source spectrum (Fig. 2a). In other words, the end-fire lobes are areas in which the phase of the correlation function of direct waves is stationary with respect to azimuth θ.

Figure 3c shows that when considering direct arrivals, the cross-correlation function is highly dependent on the source azimuth when it is computed independently for each source. When stacking the contributions of all of the sources (viz. all of the azimuths), all of the phases are averaged, and only the contributions of sources in the end-fire lobes do not vanish, where the delays are stationary. This leads to a good estimate of the actual direct-wave component of the Green's function. The average cross-correlation and the actual response as recorded in the field are compared in Figure 3d. Satisfactory reconstruction of the direct waves was achieved. Following Snieder (2004), the same approach was also proposed with the correlation of coda waves (Fig. 3b) where the scatterers play the role of virtual sources surrounding the receiver pair (Gouedard et al. 2008).

4-Mathematical results

4.1-Homogeneous body approximation

The goal of this section is to investigate the following problem theoretically: can we retrieve the Green's function between two points by performing a cross-correlation of the ambient-noise field received on those two points?

For the sake of simplicity, we will consider the scalar-wave problem for which the Green's function G is defined as the solution of the wave equation:

$$\Delta G(\vec{x};t) - \frac{1}{c^2}\frac{\partial G(\vec{x};t)}{\partial t^2} = \delta(\vec{x})\,\delta(t) \qquad (3).$$

4.1.1-The plane-wave representation in free space

From a theoretical point of view, earlier studies have investigated the problem of spatial correlation with noise fields or with wave fields obtained from a distribution of random sources. For example, this problem was studied by Aki (1957) for surface waves. He

considered the 2D case with scalar waves in a homogeneous medium from the perspective of isotropic illumination by plane waves.

The plane waves at angular frequency ω generated from sources at large distances and propagating in direction ψ are of the form:

$$u\left(\vec{r}_1;\omega\right) = F\left(\omega\right)\exp\left(ik\,\vec{r}_1.\vec{n}\right) \tag{4},$$

where $u\left(\vec{r}_1;\omega\right)$ is a displacement at position $\vec{r}_1$ of a Cartesian frame, $k = \omega/c$ is the wave number, for a plane wave incoming from the direction $\vec{n} = \left(\cos\psi, \sin\psi\right)$ with amplitude $F\left(\omega\right)$. Assuming an omni-directional distribution of incident plane waves, the field correlation between two points $\vec{r}_1$ and $\vec{r}_2$ reduces to the well-known form of a Bessel function:

$$\left\langle u(\vec{r}_1;\omega)\,u^*(\vec{r}_2;\omega)\right\rangle = \left|F\left(\omega\right)\right|^2 J_0(k\left|\vec{r}_1 - \vec{r}_2\right|) \tag{5},$$

where $J_0(k\left|\vec{r}_1 - \vec{r}_2\right|)$ is the Bessel function of the first kind and order 0. This is the essence of the spatial correlation methods proposed originally by Aki (1957), and which have been extensively used to study the structure of shallow structures.

From there, we can identify J_0 is a constituent of the 2D scalar Green's function:

$$G\left(\vec{r}_1,\vec{r}_2;\omega\right) = \frac{1}{4i}H_0^{(1)}(k\left|\vec{r}_1 - \vec{r}_2\right|) = \frac{1}{4i}\left(J_0(k\left|\vec{r}_1 - \vec{r}_2\right|) + i\,Y_0(k\left|\vec{r}_1 - \vec{r}_2\right|)\right) \tag{6},$$

where Y_0 and $H_0^{(1)}$ are the Neumann and Hankel functions of zero order.

We finally obtain:

$$\left\langle u(\vec{r}_1;\omega)\,u^*(\vec{r}_2;\omega)\right\rangle = -4\left|F\left(\omega\right)\right|^2 \mathrm{Im}\left[G(\vec{r}_1,\vec{r}_2;\omega)\right] \tag{7}.$$

As shown in Equation (7), the correlation theorem links the average correlation function (left term) to the imaginary part of the Green's function. The time domain signal

associated with $\mathrm{Im}(G)$ by Fourier transform is the causal Green's function plus its even anti-causal time-symmetrical counterpart, as shown in the next paragraph.

The generalization to the 3D free-space medium with a spatially uniform noise-source distribution is straightforward, as the field at each receiver can be decomposed as a superposition of uncorrelated plane waves from various directions. It has been established that the normalized cross-spectral density $C_{1,2}(\omega)$ at frequency ω between two receivers as 1 and 2 separated by a distance $r = |\vec{r}_1 - \vec{r}_2|$ is:

$$C_{1,2}(\omega) = \frac{\sin(kr)}{kr} \tag{8}.$$

In the time domain, the normalized correlation function is:

$$C_{1,2}(t) = \frac{1}{2\pi}\int_{-\infty}^{\infty} C_{1,2}(\omega)\exp(i\omega t)\,d\omega \tag{9},$$

which can be written as:

$$C_{1,2}(t) = \frac{1}{4\pi}\int_{-\infty}^{\infty} \frac{\exp\left[i\omega(t+r/c)\right]}{ikr}d\omega - \frac{1}{4\pi}\int_{-\infty}^{\infty} \frac{\exp\left[i\omega(t-r/c)\right]}{ikr}d\omega \tag{10}.$$

The time derivative of the correlation function is then:

$$\frac{d}{dt}C_{1,2}(t) = \frac{1}{4\pi\, r/c}\left[\delta(t+r/c) - \delta(t-r/c)\right] \tag{11}$$

The two terms in Equation (11) correspond to the backward and forward Green's function between the receivers, which demonstrates the connection between the correlation function and the Green's function.

Note that Nakahara (2006) studied in detail the relations between the spatial correlation functions and the Green's function, in 1D, 2D and 3D cases. He emphasized the dimensional character of these relations, as essentially a Hilbert transform in 2D and a differentiation in 3D.

However, the drawback of the elegant result in Equation (11) is to start from a *normalized* correlation function, with the normalization required because the overall spatial contribution from noise sources in a lossless infinite medium is infinite. Experimentally though, ambient noise signals are always finite, as is the noise correlation function. The contradiction arises as the theory is developed in lossless environments while experiments are always performed in the presence of attenuation. Thus, normalization acts as a subterfuge for avoiding the inclusion of the required attenuation in the theory.

4.1.2-Case of a homogeneous distribution of noise sources

The goal of the present section is to show how the result in Equation (11) can be derived rigorously without the need for normalization when attenuation is present in the medium.

To be as general as possible, we deal here with two receivers that are simultaneously recording ambient noise in a 3D homogeneous medium with an omni-directional and uniform distribution of noise sources. The incident field on the two receivers comes from a homogeneous spatial-temporal distribution of uncorrelated broadband noise sources. Volume attenuation is included in the medium with an attenuation parameter κ.

The Green's function between points A (in $\vec{r}_1$) and B (in $\vec{r}_2$) is then defined as follows:

$$G(\vec{r}_1,\vec{r}_2;t)=\frac{1}{2\pi}\int_{-\infty}^{+\infty}d\omega\frac{1}{4\pi|\vec{r}_2-\vec{r}_1|}\exp\left[i\omega\left(t-\frac{|\vec{r}_2-\vec{r}_1|}{c}\right)\right]\exp\left(-\kappa|\vec{r}_2-\vec{r}_1|\right) \quad (12).$$

Assuming a random spatial-temporal distribution of noise source amplitudes $S(\vec{r}_s,t_s)$, the total field received at A is:

$$P(\vec{r}_1;t)=\int_{-\infty}^{\infty}\int_{-\infty}^{t}d\vec{x}\,dt_x S(\vec{x},t_x)G(\vec{r}_1,\vec{x};t-t_x) \quad (13).$$

Here, the causality requires that the noise sources in $(\vec{x};t_x)$ that contribute to the pressure field at A at a given time t satisfy the condition $t=t_x+\frac{|\vec{r}_1-\vec{x}|}{c}$. Then the cross-correlation of the two signals recorded at A and B is defined as in Equation (1):

$$C(\vec{r}_1,\vec{r}_2;t) = C_{1,2}(t) = \frac{1}{T}\int_0^T P(\vec{r}_1;\tau)\,P(\vec{r}_2;t+\tau)\,d\tau \qquad (14).$$

$C_{1,2}(t)$ corresponds to one realization of the ambient noise cross-correlation function. To evaluate the average noise correlation function $\langle C_{1,2}(t)\rangle$ over an ensemble of realization, we use the idea that noise sources are spatially and temporally uncorrelated:

$$\langle S(\vec{x},t_x)\,S(\vec{x}',t_{x'})\rangle = Q^2\,\delta(t_x - t_{x'})\,\delta(\vec{x}-\vec{x}') \qquad (15),$$

where the notation <X> corresponds to the ensemble average of X, and Q^2 is the acoustic power of the noise sources and is taken as constant over time and space. Then it follows that:

$$\langle C_{1,2}(t)\rangle = \frac{Q^2}{64T\pi^4}\int_0^T\int_{-\infty}^{+\infty}\int_{-\infty}^{+\infty}\frac{d\tau\,d\vec{x}\,d\omega}{|\vec{r}_2-\vec{x}||\vec{r}_1-\vec{x}|}\exp\left[i\omega\left(t+\frac{|\vec{r}_1-\vec{x}|}{c}-\frac{|\vec{r}_2-\vec{x}|}{c}\right)\right] \times\exp\left[-\kappa\left(|\vec{r}_1-\vec{x}|+|\vec{r}_2-\vec{x}|\right)\right] \qquad (16).$$

Note that as written in Equation 14, τ corresponds to the running time of the signals received at A and B. The cross-correlation function $\langle C_{1,2}(t)\rangle$ is a comparison between these two signals, meaning that $\langle C_{1,2}(t)\rangle$ will extract the relative propagation times between the noise source in $\vec{x}$, and the receivers in $\vec{r}_1$ and $\vec{r}_2$. As a consequence, the integration over τ corresponds to just an accumulation of noise sources over time. In a practical experimental case, the pressure fields at A and B have first to be recorded over a finite interval time T before the cross-correlation is performed.

Assuming that the random noise sources have a creation rate n, the integral over τ is changed into the product $T\,N$. Finally, using this approach, Equation (9) becomes:

$$\langle C_{1,2}(t)\rangle = \frac{Q^2 N}{64\pi^4}\int_{-\infty}^{+\infty}\int_{-\infty}^{+\infty}\frac{d\vec{x}\,d\omega}{|\vec{r}_2-\vec{x}||\vec{r}_1-\vec{x}|}\exp\left[i\omega\left(t+\frac{|\vec{r}_1-\vec{x}|}{c}-\frac{|\vec{r}_2-\vec{x}|}{c}\right)\right] \times\exp\left[-\kappa\left(|\vec{r}_1-\vec{x}|+|\vec{r}_2-\vec{x}|\right)\right] \qquad (17).$$

Equation (16) shows that the noise correlation function in free space reduces to the calculation of a spatial integral over the noise-source locations. In the following, we show that a geometrical argument allows us to obtain an analytical solution for $\langle C_{1,2}(t)\rangle$. We first define a Cartesian coordinate system for the 3D space in which A is *(a,0,0)*, B is *(-a,0,0)*. The argument of the time-dependent exponential in Equation (17) gives a contribution to the correlation function at time t if $\vec{x}$ is such that $|\vec{r}_2 - \vec{x}| - |\vec{r}_1 - \vec{x}| = ct$.

For a time t satisfying the condition $-2a \le ct \le 2a$, the noise sources must lie on a hyperboloid (Figure 4) that will contribute to $\langle C_{1,2}(t)\rangle$ at a given time t. This implies that $\langle C_{1,2}(t)\rangle = 0$ for *t* outside the interval [-2a/c, 2a/c]. Similarly, the ellipse in Figure 4 is made of the noise sources $\vec{r}_s$ such that $|\vec{r}_2 - \vec{x}| + |\vec{r}_1 - \vec{x}| = constant$, i.e. sources that contribute to the correlation function with the same attenuation.

Figure 4. *Representation in the x-y plane of the hyperbola that contributes to a given time t in the noise-correlation function. On each hyperbola, the noise sources satisfy* $|\vec{r}_2 - \vec{x}| - |\vec{r}_1 - \vec{x}| = ct$. *For example, the horizontal axis corresponds to ct = 0. The vertical axis corresponds to ct = 2a for* $x' \ge a$, *and ct = -2a for* $x' \le -a$. *The ellipse (dashed line) represents the noise sources for which* $|\vec{r}_2 - \vec{x}| - |\vec{r}_1 - \vec{x}| = ct$, *for ct = 4a. The receivers A and B are at (a,0) and (-a,0). From Roux et al. (2005).*

Note that these conical shapes are invariant by rotation around the axis of the two receivers (Figure 4, x-axis). This means that in 3D, the hyperbola and the ellipse turn out to be a hyperboloid and an ellipsoid where the symmetry axis is the lines between the two receivers. As can be seen in Figure 2, every noise source in space belongs to a unique hyperbola.

Using a change of variable from the Cartesian coordinates to the Prolate spheroidal coordinates, it follows that:

$$\langle C_{1,2}(t)\rangle = \frac{Q^2 Nc}{64\pi\kappa}\int_{-\infty}^{+\infty} d\omega \frac{1}{i\omega}\left\{\exp\left[i\omega\left(t+\frac{2a}{c}\right)\right] - \exp\left[i\omega\left(t-\frac{2a}{c}\right)\right]\right\}\frac{\exp(-2a\kappa)}{2a} \qquad (18).$$

In the case of a medium with attenuation, the time derivative of the correlation function gives:

$$\frac{d}{dt}\left\langle C_{1,2}(t)\right\rangle = \frac{Q^2 Nc}{64\pi\kappa}\left\{\int_{-\infty}^{+\infty} d\omega \frac{1}{2a}\exp\left[i\omega\left(t+\frac{2a}{c}\right)\right]\exp(-2a\kappa) - \int_{-\infty}^{+\infty} d\omega \frac{1}{2a}\exp\left[i\omega\left(t-\frac{2a}{c}\right)\right]\exp(-2a\kappa)\right\} \quad (19).$$

The physical interpretation of Equation (19) is:

$$\frac{d}{dt}\left\langle C_{1,2}(t)\right\rangle = Q^2 N \frac{c}{2\kappa}\left[G(\vec{r}_1,\vec{r}_2;t) - G(\vec{r}_1,\vec{r}_2;-t)\right] \quad (20).$$

The amplitude term in the factor of the causal and anti-causal Green's function is made up of two contributions: (1) $Q^2 N$, which corresponds to the noise power during the recording time window *T*; and (2) the other factor $\frac{c}{2\kappa}$ is directly related to the attenuation introduced in the Green's function (Equation (12)). In section 4.3, we will see the importance of this attenuation parameter in the more general formulation of the Ward Identity. Indeed, the introduction of a small attenuation in the medium makes the correlation function converge on the noise-source spatial distribution without any constraint. Finally, the derivative of the ambient noise correlation function gives birth to the causal and anti-causal (or time-reversed) Green's functions between the two points at which the noise has been recorded.

4.2-The case of a single scatterer

We generalize the correlation theorem to the case where there is one punctual and isotropic weak scatterer in the propagation medium. The Green's function is now made up of both the direct path between the source and the receiver and the scattering contribution from the scatterer. Before a generalization to a more complex heterogeneous medium (section 4.3), the goal of this paragraph is to show how the two-point correlation function provides the two contributions of the Green's function.

The mathematical demonstration was proposed by Sato et al. (2012), who considered the scattering contribution in the first Born approximation. The Green's function $G^0(\vec{r}_1,\vec{x};\omega) = G^0_{1x}$ of the free-space medium that is the solution of the Helmoltz equation between one source in $\vec{r}_1$ and one receiver in $\vec{x}$, as:

$$\Delta G_{1x}^{0} + \left(k + i\kappa\right)^{2} G_{1x}^{0} = \delta\left(\vec{r}_1 - \vec{x}\right) \tag{21},$$

is transformed into $G\left(\vec{r}_1, \vec{x}; \omega\right) = G_{1x}$, such that:

$$\Delta G_{1x} + \left(k + i\kappa\right)^{2} G_{1x} + V_0 \delta\left(\vec{x} - \vec{y}\right) G_{1x} = \delta\left(\vec{r}_1 - \vec{x}\right) \tag{22},$$

where $\vec{y}$ is the position of the scatterer, and V_0 is the scattering coefficient.

Assuming $G_{1x} = G_{1x}^{0} + G_{1x}^{s}$, we have in the first Born approximation ($\left|G_{1x}^{s}\right| \ll \left|G_{1x}^{0}\right|$) for the scattering contribution:

$$\Delta G_{1x}^{s} + \left(k + i\kappa\right)^{2} G_{1x}^{s} = -V_0 \delta\left(\vec{x} - \vec{y}\right) G_{1x}^{0} \tag{23},$$

from which we obtain:

$$G_{1x} = -\frac{1}{4\pi r_{1x}} \exp\left[\left(ik - \kappa\right) r_{1x}\right] + V_0 \frac{\exp\left[\left(ik - \kappa\right) r_{1y}\right]}{4\pi r_{1y}} \frac{\exp\left[\left(ik - \kappa\right) r_{xy}\right]}{4\pi r_{xy}} \tag{24},$$

where $r_{1x} = \left|\vec{r}_1 - \vec{r}_x\right|$ and $r_{xy} = \left|\vec{r}_x - \vec{r}_y\right|$.

The correlation function is defined in the frequency domain as:

$$C_{1,2}(\omega) = \int_{-\infty}^{+\infty} G_{1x}^{*}(\omega) G_{2x}(\omega) d\vec{x} \tag{25},$$

with noise sources that spread to infinity. Replacing G_{1x} and G_{2x} by their expression in Equation (24), it follows from the Born approximation that:

$$C_{1,2}(\omega) = \int_{-\infty}^{+\infty} \left[G_{1x}^{0}(\omega)^{*} G_{2x}^{0}(\omega) + G_{1x}^{s}(\omega)^{*} G_{2x}^{0}(\omega) + G_{1x}^{0}(\omega)^{*} G_{2x}^{s}(\omega) \right] d\vec{x} \tag{26},$$

from which we obtain:

$$C_{1,2}(\omega) = \int_{-\infty}^{+\infty} \frac{\exp\left[\left(-ik-\kappa\right)r_{1x}\right]}{4\pi r_{1x}} \frac{\exp\left[\left(ik-\kappa\right)r_{2x}\right]}{4\pi r_{2x}} d\vec{x}$$
$$- V_0 \frac{\exp\left[\left(-ik-\kappa\right)r_{1y}\right]}{4\pi r_{1y}} \int_{-\infty}^{+\infty} \frac{\exp\left[\left(-ik-\kappa\right)r_{xy}\right]}{4\pi r_{xy}} \frac{\exp\left[\left(ik-\kappa\right)r_{2x}\right]}{4\pi r_{2x}} d\vec{x}$$
$$- V_0 \frac{\exp\left[\left(ik-\kappa\right)r_{2y}\right]}{4\pi r_{2y}} \int_{-\infty}^{+\infty} \frac{\exp\left[\left(-ik-\kappa\right)r_{1x}\right]}{4\pi r_{1x}} \frac{\exp\left[\left(ik-\kappa\right)r_{xy}\right]}{4\pi r_{xy}} d\vec{x} \quad (27).$$

Using the change of variable and the spatial integration performed in section 4.1 (from Equation (17) to Equation (18)), we have:

$$C_{1,2}(\omega) = \frac{1}{2k\kappa}\exp\left(-\kappa r_{12}\right)\frac{\sin\left(kr_{12}\right)}{4\pi r_{12}}$$
$$- V_0 \frac{\exp\left[\left(-ik-\kappa\right)r_{1y}\right]}{4\pi r_{1y}} \frac{1}{2k\kappa}\exp\left(-\kappa r_{2y}\right)\frac{\sin\left(kr_{2y}\right)}{4\pi r_{2y}}$$
$$- V_0 \frac{\exp\left[\left(ik-\kappa\right)r_{2y}\right]}{4\pi r_{2y}} \frac{1}{2k\kappa}\exp\left(-\kappa r_{1y}\right)\frac{\sin\left(kr_{1y}\right)}{4\pi r_{1y}} \quad (28),$$

which can be simplified as:

$$C_{1,2}(\omega) = \frac{1}{2k\kappa}\exp\left(-\kappa r_{12}\right)\frac{\sin\left(kr_{12}\right)}{4\pi r_{12}}$$
$$- V_0 \frac{1}{2k\kappa}\exp\left[-\kappa\left(r_{1y}+r_{2y}\right)\right]\frac{\sin\left[k\left(r_{1y}+r_{2y}\right)\right]}{4\pi r_{1y}\,4\pi r_{2y}} \quad (29).$$

We recognize in Equation (29) the part of the Green's function that is associated to the direct path between the receiver and the contribution of the scatterer. From the integral in Equation (26), it is interesting to highlight the location of the noise sources that contribute to the reconstruction of the direct path or the scatterer contribution (Figure 5). As well as the end-

fire lobe that defines the angle interval in which noise sources coherently contribute to the direct path of the Green's function (Figure 5, red), there are new angle intervals associated to the coherent contribution of the scattered field (Figure 5, blue). As the path length of the scattered ray is longer than the A-to-B direct path, the width of this beam is smaller than the end-fire lobe.

Figure 5. *Schematic representation of the end-fire lobes (red) associated to the coherent contribution of noise sources (gray dots in the background) to the correlation function between two receivers at A and B. The part of the Green's function associated to the scatterer (blue square) is reconstructed from noise sources located in different beams (blue). For the sake of clarity, the dashed lines (red and blue) represent the direct and scattered ray paths, respectively.*

Taking into account the Green's function formulation in Equation (24), we finally have:

$$C_{1,2}(\omega) = \frac{c}{2i\omega\kappa}\,\mathrm{Im}\left[G_{12}(\omega)\right] \qquad (30).$$

Recognizing the time-derivative as the $i\omega$ term at the denominator in Equation (30), it follows that the correlation theorem is still valid for a medium with one local heterogeneity. Note that an extension of the plane-wave approach has also been performed in the presence of a scatterer (Sanchez-Sesma et al. 2006).

Following the same mathematical approach as in Equations (23) to (29), Sato et al. (2012) extended this result to a set of scatterers in the Born approximation. Finally, Margerin and Sato (2012) went one step further, showing that all of the scattering orders in the Dyson's equation (including multiple scattering) can be taken into account in the correlation function for the same result as in Equation (30).

4.3-Arbitrary heterogeneous medium

We now generalize the correlation theorem to the case of scalar waves propagating in any heterogeneous medium. This approach was first developed by Weaver et al. (2004) and then

by Snieder (2007). It indicates the role of attenuation in the connection between the correlation function and the Green's function.

We start from the Helmholtz equation that defines the Green's function $G_{1x} = G(\vec{r}_1, \vec{x}; \omega)$ for scalar waves in a heterogeneous medium at frequency ω:

$$\Delta G_{1x} + V(\vec{x}) G_{1x} + (k + i\kappa)^2 G_{1x} = \delta(\vec{x} - \vec{r}_1) \quad (31).$$

where the potential $V(\vec{x})$ describes the scattering contribution to the wavefield that is assumed to be finite in space, meaning that it does not extend to infinity.

Using two points in $\vec{r}_1$ and $\vec{r}_2$, we define the flux of the Poynting vector through a closed surface S located far away from any medium heterogeneity as:

$$I = \oint_S \left[G_{1x} \vec{\nabla}(G_{2x}^*) - \vec{\nabla}(G_{2x}) G_{1x}^* \right] \overrightarrow{dS} \quad (32).$$

Using the divergence theorem, we can transform this flux integral into a volume integral $\mathcal{V}$:

$$I = \int_{\mathcal{V}} \vec{\nabla} \left[G_{1x} \vec{\nabla}(G_{2x}^*) - \vec{\nabla}(G_{1x}) G_{2x}^* \right] dV \quad (33).$$

This can be simplified into:

$$I = \int_{\mathcal{V}} \left(G_{1x} \Delta G_{2x}^* - \Delta G_{1x} G_{2x}^* \right) dV \quad (34).$$

From Equation (31), we have:

$$\Delta G_{2x}^* = \delta(\vec{x} - \vec{r}_2) - V(\vec{x}) G_{2x}^* - (k - i\kappa)^2 G_{2x}^* \quad (35),$$

$$\Delta G_{1x} = \delta(\vec{x} - \vec{r}_1) - V(\vec{x}) G_{1x} - (k + i\kappa)^2 G_{1x} \quad (36),$$

which assumes that the potential $V(\vec{x})$ is real. Physically speaking, this means that there is no vortex or flow in the medium that would break the spatial reciprocity theorem.

Combining Equations (35) and (36) into Equation (34), it follows that:

$$I = G_{12} - G_{21}^{*} - \frac{4i\omega\kappa}{c}\int_{\mathcal{V}} G_{1x}G_{2x}^{*}\,dV \qquad (37).$$

Finally, using Equations (32) and (37), and taking into account that $G_{12} = G_{21}$, due to the reciprocity theorem, we can conclude that:

$$G_{12} - G_{12}^{*} = \frac{4i\omega\kappa}{c}\int_{\mathcal{V}} G_{1x}G_{2x}^{*}\,dV + \oint_{S}\left[G_{1x}\vec{\nabla}\left(G_{2x}^{*}\right) - \vec{\nabla}\left(G_{1x}\right)G_{2x}^{*}\right]\overrightarrow{dS} \qquad (38).$$

In Equation (38), the left-hand side corresponds to the causal and anti-causal Green's function. Using an equivalent formulation (see paragraph 4.3.3) of the representation theorem, Snieder (2007) detailed the different contributions of the volume and surface integrals in a simple configuration. For sake of simplicity, we propose to separately examine the volume and surface integrals in the two following cases.

4.3.1-If the attenuation parameter $\kappa \neq 0$

In the case where the attenuation parameter $\kappa \neq 0$, we make the choice to extend the volume $\mathcal{V}$ to infinity. This means that the volume integral over the 'noise sources' x spreads over infinity. The product $G_{1x}G_{2x}^{*}$ corresponds to the correlation between the field received in $\vec{r}_1$ and $\vec{r}_2$ from a source in $\vec{x}$. Far from the medium heterogeneities, the Green's function decreases as:

$$\left|G_{1x}\right| \sim \frac{1}{4\pi\left|\vec{x} - \vec{r}_1\right|}\exp\left(-\kappa\left|\vec{x} - \vec{r}_1\right|\right) \qquad (39).$$

Then, we have in the far field, with $\left|\vec{x}\right| \gg \left|\vec{r}_1\right|, \left|\vec{r}_2\right|$:

$$\left|G_{1x}\vec{\nabla}\left(G_{2x}^{*}\right)\right| \sim \left|\vec{\nabla}\left(G_{1x}\right)G_{2x}^{*}\right| \sim \frac{k^2}{16\pi^2\left|\vec{x}-\vec{r}_1\right|\left|\vec{x}-\vec{r}_2\right|}\exp\left[-\kappa\left(\left|\vec{x}-\vec{r}_1\right|+\left|\vec{x}-\vec{r}_2\right|\right)\right] \qquad (40),$$

such that $\oint_S\left[G_{1x}\vec{\nabla}\left(G_{2x}^{*}\right)-\vec{\nabla}\left(G_{1x}\right)G_{2x}^{*}\right]\overrightarrow{dS} \to 0$ even when the surface S expands to infinity, because of the exponential decrease due to attenuation.

We then obtain:

$$G_{12}-G_{12}^{*} = \frac{4i\omega\kappa}{c}\int_{\vec{V}} G_{1x}G_{2x}^{*}\,dV \qquad (41),$$

which has sometimes been defined as the Ward Identity in the recent literature.

Equation (41) is the generalization of Equations (20) and (30) to any heterogeneous medium in the presence of attenuation. As in Equation (30), note that the $i\omega$ term on the right-hand side corresponds to the time-derivative of the correlation function. As shown in the above equations, the attenuation parameter κ is a key parameter in the Ward Identity. Physically speaking, the attenuation manages to balance the energy flux in the system. Another interpretation of the attenuation is related to the thermodynamic equilibrium as defined through the fluctuation-dissipation theorem.

4.3.2-If the attenuation parameter $\kappa = 0$

In the case where the attenuation parameter $\kappa = 0$, Equation (38) simplifies into:

$$G_{12}-G_{12}^{*} = \oint_S\left[G_{1x}\vec{\nabla}\left(G_{2x}^{*}\right)-\vec{\nabla}\left(G_{1x}\right)G_{2x}^{*}\right]\overrightarrow{dS} \qquad (42).$$

In Equation (42), the sources are only present on the closed surface S, and no source is present in the volume. If the surface is taken in the far field of the medium heterogeneities, for every point x on the surface S, we have:

$$G_{1x} \sim \frac{1}{4\pi\left|\vec{x}-\vec{r}_1\right|}\exp\left(-ik\left|\vec{x}-\vec{r}_1\right|\right) \text{ and } \vec{\nabla}\left(G_{1x}\right) \sim i\vec{k}\,G_{1x}, \qquad (43)$$

from which it follows that:

$$G_{12} - G_{12}^{*} = -2i\frac{\omega}{c}\oint_S G_{1x} G_{2x}^{*}\, dS \qquad (44).$$

where the right-hand side corresponds to the correlation function calculated for sources located on the surface S. As previously, the $i\omega$ term refers to the time-derivative of the correlation function.

The last formulation of the correlation theorem is appealing for geophysicists that usually deal with noise sources at the Earth surface. However, according to Equation (44), the surface must surround the receiving points in $\vec{r}_1$ and $\vec{r}_2$, which never happens in practice. Note also that the approximation $\kappa = 0$ is not valid in most practical cases.

4.3.3-Another formulation of the correlation theorem

In the literature on ambient noise correlation, Equation (44) is classically defined as one formulation of the representation theorem, and a different mathematical expression is sometimes used [Wapenaar, 2004; Wapenaar and Fokkema, 2006; Godin, 2007]:

$$\tilde{G}_{12} + \tilde{G}_{12}^{*} = \frac{2}{c}\oint_S \tilde{G}_{1x} \tilde{G}_{2x}^{*}\, dS \qquad (45).$$

Compared to Equation (44), this other formulation of Equation (45) connects the summation of the causal and anti-causal Green's function to the correlation function without the time derivative. It is important to understand that the two expressions in Equations (44) and (45) are equivalent. Indeed, Equation (45) is obtained from a different definition of the Green's function (see Equation (31) for comparison):

$$\Delta\tilde{G}_{1x} + V(\vec{x})\tilde{G}_{1x} + (k + i\kappa)^2 \tilde{G}_{1x} = i\omega\delta(\vec{x} - \vec{a}) \qquad (46),$$

this only differs in the source term on the right-hand side, which corresponds to a ‘mass injection’ in Equation (46) when the Green's function definition in Equation (31) refers to a ‘momentum injection’.

Finally, some authors have dealt with the case of a complex potential $V(\vec{x})$, which would correspond, for example, to the presence of a vorticity field or a flow that breaks the condition of spatial reciprocity in the propagation medium. It appears then that the correlation function is no longer symmetric in time. The travel-time associated to the causal part can then be different from the travel-time of the anti-causal part, as the Green's function from one receiver to the other is not equivalent to the Green's function along the reverse path [Wapenaar, 2006].

Note also that Colin de Verdière (2009, 2011) proposed a very general and quite mathematical approach where the wave propagator is simply defined as a self-adjoint differential operator. Including attenuation and taking into account any type of scattering in the wave equation for a homogeneous noise distribution, he retrieved the same connection between the correlation function and the causal/ anti-causal Green's function (Equations (20) and (41)).

4.4-Modal approach in finite bodies

Up to this point, we have presented the formulation of the correlation theorem in open homogeneous or heterogeneous media. However, the first theoretical and experimental demonstration of the convergence of the correlation function towards the Green's function was performed in finite bodies in which the wave propagation is described from a modal approach [Weaver and Lobkis (2001)].

For sake of simplicity, we deal with a 1D finite body, in which the Green's function can be written as an expansion in terms of the normal modes $U_n(x)$:

$$G(x_1, x_2; t) = c^2 \sum_n U_n(x_1) U_n(x_2) \frac{\sin(\omega_n t)}{\omega_n} \Theta(t), \qquad (47)$$

where ω_n correspond to the eigenfrequency of mode n and $\Theta(t)$ is the Heaviside function that is necessary to respect the causality of the Green's function.

When uncorrelated noise sources are uniformly distributed in the volume V of the finite body, the correlation function between two receivers at x_1 and x_2 can be written as:

$$C_{1,2}(t) = \frac{1}{T}\int_0^T d\tau \int_V dx\, G(x_1, x; \tau) G(x_2, x; t+\tau) \tag{48}$$

From Equation (47), it follows that:

$$C_{1,2}(t) = \frac{c^4}{T}\int_0^T d\tau \int_V dx \sum_m \sum_n U_n(x_1) U_n(x) U_m(x_2) U_m(x) \frac{\sin(\omega_n \tau)}{\omega_n} \frac{\sin\left[\omega_m (t+\tau)\right]}{\omega_m} \tag{49}$$

Using the orthonormality relation between modes:

$$\int_0^L dx\, U_n(x) U_m(x) = \delta_{nm}, \tag{50},$$

we have:

$$C_{1,2}(t) = \frac{c^4}{T}\sum_n \frac{1}{\omega_n^2} U_n(x_1) U_n(x_2) \int_0^T \sin(\omega_n \tau) \sin\left[\omega_n (t+\tau)\right] d\tau \tag{51}.$$

When the recording window T is long compared to the largest period of the excited modes ($T \gg 1/\omega_n$, $\forall n$), it follows that:

$$C_{1,2}(t) = \frac{c^4}{2}\sum_n U_n(x_1) U_n(x_2) \frac{\cos(\omega_n t)}{\omega_n^2} \tag{52},$$

and then:

$$\frac{d}{dt} C_{1,2}(t) = -\frac{c^4}{2}\sum_n U_n(x_1) U_n(x_2) \frac{\sin(\omega_n t)}{\omega_n} = -\frac{c^2}{4}\left[G(x_1, x_2; t) - G(x_1, x_2; -t)\right] \tag{53}.$$

As expected, the physics of the correlation theorem also applies to the modal formulation. As well as the thermal diffuse-noise experiment achieved by Weaver and Lobkis (2001) in a sample of duralumin, other demonstrations have been performed in bounded

media. For example, acoustic propagation in underwater waveguides is bounded by the air-water and water-bottom interfaces that justify the presence of propagating modes. Different authors have studied the convergence of the correlation function towards the Green's function in underwater acoustics, with some successful applications to array element synchronization or bottom mapping.

4.5-Equipartition and random fields

As the Earth is a complex medium, scattering by small-scale heterogeneities is a relevant phenomenon to understand seismic-wave propagation, particularly for short period waves in the lithosphere. Scattering is revealed at the first order by the amplitude decay of the direct arrivals and by the long coda of seismograms. For coda waves, multiple scattering must be taken into account. This is a general issue in different domains that has led to considerable developments that were aimed at the quantitative description of the spatial and temporal evolution of the local energy, or intensity, of the scattered field, via the diffusion approximation or the more general radiative-transfer equation (see Sato et al. 2012, for a review on seismic waves). While the average energy density is successfully predicted by these theories, the phases, i.e., the details of the wave shapes, are assumed to be unpredictable random variables. At the same time, the deterministic phase of the waves that is neglected in the theory for energy or intensity is clearly expressed in phenomena like coherent back scattering (Larose et al. 2004) and long-range correlations in the form of the Green's function (Campillo and Paul 2003).

For waves propagating in the heterogeneous Earth, the diffusive regime emerges after several scatterings at a time that depends on the scattering strength of the medium (e.g., Sato et al. 2012). Asymptotically for large times, the wavefield is expected to consist of random contributions of all of the possible modes of propagation, with equal weights on average (e.g., Weaver 1982, Ryzhik et al. 1996). This state is referred to as equipartition. Note that we refer here to the modes of a fictitious model close enough to the actual complex Earth to essentially share the same propagation properties (e.g., Campillo and Margerin 2010). In a realistic medium, the propagation modes are associated with complex eigenfunctions. Equipartition, therefore, does not imply that their contributions are the same everywhere. At a given observation point, equipartition results in a constant ratio of the relative contributions of the P-waves and S-waves to the time-dependent diffuse local energy, independent of the detail of the scattering. The stabilization of the S-to-P energy ratio is observed in the coda of actual seismograms (Hennino et al. 2001, Margerin et al. 2009, Yamamoto et al. 2011). This is a

good indication that the wavefield entered into a regime where the diffusion approximation can be applied to describe the average energy density.

Equipartition and isotropy are asymptotic states of diffuse fields for large lapse times. Indeed these conditions are generally not reached in practice. In the presence of a single source, the overall divergent flux of energy precludes a perfect isotropy of the flux even for large lapse times. It must be noted that although it is an indicator of the diffusion, the stabilization of the energy ratios is not synonymous with equipartition, and therefore isotropy of specific intensity (Paul et al. 2005).

We recast here a plausibility argument for the construction of Green's function from correlation of diffuse fields that was originally proposed by Lobkis and Weaver (2001). In the case of a finite body, a diffuse field can be expressed in terms of the normal modes $U_n(\vec{r})$ as:

$$\phi(\vec{r};t) = \sum_n a_n U_n(\vec{r}) \cos(\omega_n t) \qquad (54),$$

where the complex amplitudes a_n are uncorrelated random variables, such that:

$$< a_n a_m^* >= F(\omega_n)\delta_{nm} \qquad (55).$$

where F(ω)governs the shape of the spectral energy density. The cross correlation of the two fields at points $\vec{r}_1$ and $\vec{r}_2$ is:

$$C_{1,2}(t) = \frac{1}{T}\int_0^T \phi(\vec{r}_1,\tau)\phi(\vec{r}_2,t+\tau)d\tau \qquad (56).$$

Assuming a long recording interval *T*, this reduces to:

$$C_{1,2}(t) = \frac{1}{2}\sum_n F(\omega_n)U_n(\vec{r}_1)U_n(\vec{r}_2)\cos(\omega_n t) \qquad (57).$$

This expression of the correlation function must be compared to the Green's Function:

$$G(\vec{r}_1,\vec{r}_2;t)=\sum_n U_n(\vec{r}_1)U_n(\vec{r}_2)\frac{\sin(\omega_n t)}{\omega_n}\Theta(t) \qquad (58).$$

For positive times, $C_{1,2}(t)$ and $G(\vec{r}_1,\vec{r}_2;t)$ only differ by a time derivation and the spectrum of the diffuse field. While limited to the case of finite bodies, this simple demonstration is a justification for the pioneering experiments performed in acoustics by Lobkis and Weaver (2001).

4.6-Example with elastic waves

In the homogeneous 2D case with surface waves discussed in section 4.1.1, the wavefield is projected on plane waves that propagate in every direction with constant amplitude. The equipartition then reduces to isotropy. The correlation of equipartioned field at two points therefore reduces to the case discussed in section 4.1. The elastic case is more informative.

In the elastic 2D case, the equation of motion for the velocity vector $\vec{u}$ is:

$$\beta^2\frac{\partial^2 u_i}{\partial^2 x_j}+\left(\alpha^2-\beta^2\right)\frac{\partial^2 u_j}{\partial x_i \partial x_j}=\frac{\partial^2 u_i}{\partial^2 t} \qquad (59),$$

where u_i is one component of the velocity vector, and α and β correspond to the P-wave and S-wave velocities, respectively.

Assuming a homogeneous medium, we project the elastic wavefield on the P and S plane waves. For the 2D case, the ratio of S-wave to P-wave energies of an equipartioned field can be obtained by a simple mode-counting argument:

$$\frac{E_S}{E_P}=\frac{\alpha^2}{\beta^2} \qquad (60).$$

Let us consider an isotropic 2D field in which P-waves and S-waves are propagating in all directions, with spectral densities S^2 and P^2 independent of the direction of propagation. We denote by $\vec{q}$ and $\vec{k}$ the wavenumber for the P-waves and S-waves, respectively.

Following Sanchez-Sesma and Campillo (2006), we assume an energy ratio between

the S-waves and P-waves such that: $\varepsilon \frac{E_S}{E_P} = \frac{\alpha^2}{\beta^2}$ with $\varepsilon = 1$ for equipartition. We consider the cross-correlation of the resulting field $\vec{u}$ at positions $\vec{x}$ and $\vec{y}$. We assume $\vec{y}$ to be at the origin. Position $\vec{x}$ is written as $\left(x_1 = r\,\gamma_1, x_2 = r\,\gamma_2\right)$. After averaging over the incidence direction for an isotropic plane wave distribution, the correlation can be written as:

$$\left\langle u_i\left(\vec{y};\omega\right) u_j^*\left(\vec{x};\omega\right)\right\rangle = \frac{S^2\beta^2}{2}\left[A\delta_{ij} - B\left(2\gamma_i\gamma_j - \delta_{ij}\right)\right] \qquad (61),$$

where,

$$A = \varepsilon\frac{J_0\left(|\vec{q}|r\right)}{\alpha^2} + \frac{J_0\left(|\vec{k}|r\right)}{\beta^2};\; B = \varepsilon\frac{J_2\left(|\vec{q}|r\right)}{\alpha^2} - \frac{J_2\left(|\vec{k}|r\right)}{\beta^2} \qquad (62).$$

When the equipartion energy ratio is assumed, i.e., $\varepsilon = 1$ in Equation (60), we recognize the exact compact form of the 2D elastic Green's function, and the cross correlation is simply given by (Sanchez-Sesma and Campillo 2006):

$$\left\langle u_i\left(\vec{y};\omega\right) u_j^*\left(\vec{x};\omega\right)\right\rangle = -8E_S\,k^{-2}\,\mathrm{Im}\left[G_{ij}\left(\vec{x},\vec{y};\omega\right)\right] \qquad (63),$$

where $E_S = \rho\omega^2\,S^2/2$.

Note that in the present case, we use the definition of the Green's function for the elastodynamic equation (Equation (59)) as the response in the displacement to a unit force. This simple canonical case can be extended to 3D and illustrates the close relations between equipartition of the wavefield and the extraction of the Green's function from the cross correlations.

In the literature, different definitions of the equipartition are presented that can depend on: (1) the use of a time-domain or frequency-domain approach; (2) the properties of the propagation medium (open or bounded medium, presence of scatterers); and (3) the nature of the incident wavefield (stationary random noise, spatial distribution of pulsed sources, plane waves or modal excitations). Even though equipartitioning is at the basis of the noise correlation theorem, all situations are not equivalent. For example, we will consider in the

next paragraphs and in practical applications some cases where parts of the Green's function can be extracted in the absence of equipartitioning.

5-Practical limitations

5.1-Partial focusing

We have seen that the correlation of an even distribution of sources can lead to the Green's function of the medium. Indeed in the actual application of ambient-noise correlation, the sources are likely to result in a form of non-isotropy of the incoming flux to the pair of stations of interest. In this case, it cannot be expected that the exact response of the Earth will be retrieved. It is important to determine how an improper distribution of the source affects the cross-correlation, and how reliable the measurements of travel-times or of amplitude become.

We start with an intuitive argument that follows the time-reversal analogy presented in the Introduction. Figure 6a shows a numerical test similar to that in Figure 1, except for the distribution of the sources. The sources are now located along a segment (Figure 6a), which offers poor azimuthal coverage of the medium. The presence of scattering partly compensates for this uneven distribution of the sources. We now observe relatively poor focusing and a clearly different pattern for snapshots at positive and negative times. Figure 6 illustrates clearly the impact of the physical flux of energy on the reconstruction. The reconstructed Green's function does not show the expected temporal symmetry. Furthermore, for receiver pairs oriented perpendicular to the flux, there is no detectable trace of the propagating wave.

In general, it is therefore clear that correlations of noise cannot be considered directly as actual Green's functions for imaging purposes. The distribution of the noise sources has to be considered as a constituent of observables, such as arrival times or amplitudes. This can be formulated explicitly for a general imaging approach in the expression of the sensitivity kernels for noise correlations (Tromp et al. 2010, Hasanoge 2013)). In practice, the space-time distribution of the noise sources is not known precisely. With simple assumptions, it is nevertheless possible to quantitatively determine the bias between noise correlations and true Green's functions.

Figure 6. *Snapshots of cross correlations with respect to the field at the center (+), as in Figure 1 but with a distribution of sources limited to a line ((a), x symbols). (b), (c) and (d) correspond to correlation times of -30 s, 0 s and 30 s.*

5.2-Travel-time measurements

Even when a propagating wave is identified, it is important to quantitatively evaluate the quality of the measurements that can be performed when the distribution of sources leads to nonisotropic illumination of the station pairs. Let us consider a simple 2D case, where a pair of stations is surrounded by a distant distribution of incoherent sources that leads to nonisotropic specific intensity (Weaver et al. 2009). This is a geometry of interest when dealing with surface waves from distant noise sources (Tsai, 2009).

We assume that we measured the derivative of the correlation between the signal observed at the two receivers over the angle θ between the direction of incidence and the strike of the two receivers (Fig. 3c). $B(\theta)$ is the azimuthal distribution of the energy of the sources, and it can be expanded as:

$$B(\theta) = B_0 + B_1 \cos\theta + B_2 \cos 2\theta + ... \tag{64}$$

Note that only even terms contribute to this problem, because of the symmetry of the apparent velocity with respect to $\theta = 0$. Let us consider the case of distant receivers, i.e., *kx >>1*. We are in the high frequency limit where the contributions to the correlations are dominated by the contributions of the end-fire lobes, i.e., $\theta \simeq 0$. The goal is to evaluate the time error that is induced by the anisotropy of the sources. To be under conditions useful to seismological applications, the induced bias (delay) δt is evaluated as the time of the maximum of the cross-correlation between a Gaussian pulse of central frequency ω_0 in the isotropic source ideal case ($B(\theta) \equiv 1$) and that of the nonisotropic case. Under the high-frequency approximation, it can be shown that (Weaver et al, 2009):

$$\delta t = \frac{B''(\theta = 0)}{2t\,\omega_0^2\, B(\theta = 0)} \tag{65}$$

where $B''(\theta)$ refers to the second-order derivative of $B(\theta)$.

These formulae indicate that the error decays with frequency and with interstation distance. This is in agreement with the conclusion of Yao and van der Hilst (2009). The decay of the bias with interstation distance can be understood as the diminution of the angular size of the end-fire lobes with increasing distance.

The stationary phase theorem helps in the interpretation of the physics aspect of this observation (see section 3.2). Only the sources almost in the alignment of the receivers can contribute to the reconstruction. The aperture of the zone where the coherent sources are located varies with the square root of the ratio between the wavelength and the distance between the receivers. At higher frequencies, the end-fire lobes are narrower (Roux et al. 2004, Spetzler and Snieder 2004, Larose 2005) and the correction term is smaller. For simplicity, we have discussed here only the positive correlation time, but the argument is the same for negative time, and a formula similar to Equation (65) is obtained with direction π instead of 0.

Figure 7. *Bias in travel-time measurements for a source amplitude distribution of the form B. Different values of B_2 then correspond to different source intensity distributions. (a) Shape of the azimuthal distribution for B_2 = 0 (left panel, isotropic distribution) and B_2 = -0.6 (right panel, anisotropic distribution). (b) Correlations of direct waves as defined in Figure 3(b). Measured (crosses) and predicted (dashed line) relative time shifts for B_2 ranging from 0 to -0.6. The theoretical values result from Equation (65). Error bars correspond to standard deviations of 18-pair measurements. The reference travel-time corresponds to the correlation function obtained for an isotropic distribution of sources. (c) The same measurements as in (b), but with cross-correlations of time windows that correspond to coda waves (Figure 3(b)).*

These formulae have been validated numerically and experimentally. Froment et al. (2011) used actual Green's functions obtained during the seismic exploration experiment that was presented in section 3.2 (Figure 3), and they found excellent agreement between observation and theory. This is illustrated in Figure 7, which shows the evolution of the travel-time bias with increasing anisotropy of the incoming field. The anisotropy of intensity is produced by a modulation of the amplitude of individual source records of the form $B(\theta) = 1 + B_2 \cos(2\theta)$, where θ is defined as in the insert of Figure 3b. B_2 varies from 0 (isotropy) to -0.6. The two extreme cases are plotted in Figure 7a. To be under the conditions of the theoretical formula (Equation (65)), the correlations are computed for the direct waves (Figure 3b), weighted according to $B(\theta)$ for each source, and then averaged over the set of sources. Figure 7b shows the very good agreement between the theoretical expectations given by Equation (65) and the actual measurements.

5.3-Amplitude and spreading

When the conditions for the perfect reconstruction of the Green's function are fulfilled, the amplitude of correlation can be used to study the attenuation properties along the path, or the local amplification produced by specific local geological structures. In Figure 6, we show how an uneven distribution of sources results in poor focusing in a simple medium for a scalar problem. It is noticeable that poor focusing means that the natural curvature of the Green's function wave front is not correctly reconstructed, and that consequently the geometrical decay of amplitude is not reproduced. In general cases, it is dangerous to mix noise cross-correlations for pairs in different azimuths to retrieve the attenuation properties of the crust.

The simplest case of the illumination by a plane illustrates the specific difficulty associated with decay measurements. This occurs when a strong localized source is acting far away from the two receivers. If the noise includes such a predominant plane wave propagating in the direction of the two receivers, the cross-correlation is not the Green's function, although the time of transport of energy is the same, even if the phase is not retrieved correctly (see section 4.1). The effect is obviously much more severe for the amplitude, as the plane wave has no geometrical spreading, in contrast to the Green's function. Attenuation measurements would be strongly biased by this effect, which cannot be corrected by energy normalization (e.g., Gouédard et al. 2008).

It was nevertheless convincingly showed by Prieto et al. (2009) and Lawrence and Prieto (2011) that attenuation studies can be performed with ambient noise. These authors used the coherency, a normalized version of the cross-correlation, in place of correlation (see Section 6 below). A discussion of the feasibility and limitations of attenuation studies with ambient noise is presented in Prieto et al. (2011) and Weemstra et al. (2013).

Considering only the reconstruction of the direct waves in the scalar case can hide some difficulties that arise in practical applications, with ambient noise or with active sources at the surface. In the presence of several waves (P and S, reflections) and imperfect illumination, the correlation can show pulses associated to stationary-phase conditions, but not to physical arrivals. These spurious arrivals correspond to correlation times of waves of different natures; i.e., which are not propagating between the two points of observations. For a distribution of sources at the surface, Snieder et al. (2006) give an example of interest for exploration. They considered a simplified case with two reflections at different depths. When considered as a function of the position of the source, the difference in travel-time between the two reflected waves at the receivers had a maximum at a finite distance. According to the stationary-phase argument, a spurious arrival can therefore be expected at a time that is

actually a difference of travel-time between the reflector levels at depth, without significance for the actual paths between the receivers. Indeed, this problem vanishes if the source distribution extents at depth, or if scatterers acting as sources mimic an even distribution of sources.

5.4-Influence of scattering

Although it is impossible to directly separate the contributions of direct and scattered waves in the ambient noise produced by a distribution of uncorrelated sources, we can easily evaluate the behavior of the correlation of scattered waves in the experiment presented in section 5.2 and in Figure 7. The results of Figure 7b, which were obtained with direct waves, were repeated for the correlation of coda windows as defined in Figure 3b. The resulting measurements are presented in Figure 7c as a function of the anisotropy coefficient B_2. The bias in travel-time observed for coda-wave correlations is much smaller than for the case of direct waves. In the worst case, i.e., $B_2 = -0.6$, $\delta t / t$ only reaches 2×10^{-3}. This is due to the smooth azimuthal distribution of the intensity of the coda waves. This shows the important part played by scattered waves for the effectiveness of the correlation method.

6-Processing

6.1-Processing and convergence

The basic expectation when correlating noise time series is that for long times of observation, the noise source distribution is averaged towards a distribution that is acceptable with respect to the mathematical requisites discussed in section 4. An obvious difficulty is the presence of strong energy transients that potentially dominate in the correlation. Those transients can be large earthquakes, local storms in the microseism spectral band or various other sources depending on the frequency range considered. Different strategies are used to improve the temporal stationary of the records before correlation.

The first possibility is to remove the time windows with earthquakes. This can be done from earthquake bulletins, at least for large events. In practice, a detection algorithm is required to identify small events if no further normalization is applied.

Indeed strong direct waves generally contribute to nonphysical signals in the correlation. On the other hand, the scattered waves of the coda are a valuable contribution to the reconstruction of the Green's function. As the duration of the coda is much longer than

that of the direct waves, efficient processing consists of the normalization of the signal. This normalization is necessary in most cases, even after earthquake rejection.

One-bit normalization was used for the correlation of seismic codas by Campillo and Paul (2003), to balance the temporal exponential decay of the intensity in the coda. This was then used in numerous studies on noise correlation (e.g., Shapiro and Campillo 2004, Shapiro et al. 2005, Cupillard et al., 2011). That the correlation function of two hardly clipped signals is very close to that of the original signals has been discussed in detail in communication theory (e.g. van Vleck and Middleton 1966). The numerical simulations of Cupillard and Capdeville (2010) showed that even geometrical spreading and attenuation can be retrieved from correlations of 1-bit clipped data. Instead of using 1-bit correlation, Sabra et al. (2005) introduced a clipping procedure to limit the contribution of high-amplitude transients, while leaving the background noise unaffected. Bensen et al. (2007) proposed to apply a running-average procedure to ensure the temporal stationarity.

Instead of affecting the data by a form of nonlinear processing, Prieto et al. (2011) and Poli et al. (2012a) proposed to use short time windows, as short as 1 h, to compute the correlation. Transients can be removed after statistical analysis of the total energy of the signal in all of the windows. Each correlation is normalized according to its energy before stacking.

Sabra et al. (2004) analyzed the quality of the reconstruction for a set of station pairs within a range of 180 km to 220 km in Southern California, USA. As shown in Figure 8a, the cross-correlations are relatively stable over time, as seen for each day of July 2004 for a single station pair. While there are some fluctuations in the small-amplitude waveforms, the main arrivals are stable. The SNRs for each day and each station pair show moderate variations as the noise and seismicity varies. We sum the cross-correlation time series for each day to obtain the time series for N number of days and to compute the SNR (Figure 8b). Each day is treated as an independent observation, and therefore for each N the sum is computed for all of the combinations of the 18 days. The accumulated SNR based on the summed traces shows clearly that the SNR increases in proportion to the square root of the recording time, in agreement with Sabra et al. (2005a) and Snieder (2004).

Figure 8. *(a) Estimated noise correlation function for one station pair at a distant of 182 km, for each day of July. The summed trace for the whole month of July is shown as the thick solid line. (b) Mean and standard deviations of the SNR (in dB scale) computed by summing all of*

the combinations of the correlation functions over a number of days. The square root dependence is shown as a dotted line (from Sabra et al. 2005a).

Larose et al. (2008) studied the role of scattering in the convergence towards the Green's function. In this context, the SNR is the ratio between the level of signal in the correlations and the level of remnant fluctuations. They analyzed the SNR dependence in the context of a discrete random distribution of noise sources in a scattering medium. Indeed the SNR increases with the number of sources. When scattering is present, the SNR increases with scattering strength. This is due to the increase in the duration of the individual source signals with stronger scattering, in addition to the previously discussed isotropization of the intensity. Disorder here improves the quality of the reconstruction. On the contrary, the SNR is directly dependent on the amplitude of the actual Green's function. The amplitude decreases with travel-time or distance, and it is sensitive to scattering and absorption.

As the ambient noise spectrum in the microseism band shows clear peaks, it is convenient to introduce spectral whitening (e.g., Bensen 2007). With the nature of a seismogram as non-stationary, it is natural to introduce multidimensional filtering to de-noise the correlations. Adaptive filtering based on the S transform (Stockwell et al. 1996) was used by Baig et al. (2009), while Schimmel et al. (2011) proposed the use of instantaneous phase coherence to weigh the stack of individual correlations.

Stehly et al. (2011) used filters in the curvelet transform space to improve the SNR of stacked correlations. The previous approaches were based on the use of signal-processing tools. A physics-based approach can be expected to improve the reconstruction. In the noise-correlation context, this consists of minimizing the effects of the nonisotropic illumination. This was done by using an optimization scheme, which was referred to as multidimensional deconvolution by Wapenaar et al. (2008), or as a passive inverse filter by Gallot et al. (2011).

Velocity measurements and the evaluation of their uncertainties can be improved by using the nine correlations obtained with three-component records, with each correlation being defined for positive and negative times. The correlation matrix is expected to show the symmetry of the Green's tensor (e.g., Campillo and Paul 2003, Sabra et al. 2005). For practical applications, the computation of the complete correlation matrix allows redundant measurements to be made of Rayleigh wave velocities and their variance (e.g., Stehly et al. 2010).

6.2-Correlation of correlations

We have seen that the cross-correlation function of long ambient-noise time series can be identified as the sum of the causal and acausal Green's function. So far, we have discussed the reconstruction of ballistic arrivals. The Green's function also contains the late arrivals associated with scattered waves. According to the discussion in section 4, we expect these arrivals to also be present in the noise cross-correlations, as has been verified with numerical simulations (e.g., Derode et al. 2003). In the ideal case, the later part of the noise correlation should contain the coda part of the Green's function, and it might be possible to correlate these waves as we correlate standard earthquake codas, to reconstruct the Green's function (Campillo and Paul 2003). This is the concept of the so-called C^3 method; i.e., re-**c**orrelating the **c**oda of the noise-**c**orrelation functions to reconstruct the Green's function (Stehly et al. 2008, Froment et al. 2011, Ma and Beroza 2012). Garnier and Papanicolaou (2009) demonstrated the validity of this method based upon stationary-phase analysis of the C^3 function leading terms, and they confirmed that this method can enhance the quality of travel-time estimates in the case of anisotropic source distributions.

Figure 9. *From the noise correlations (C1) to the correlation of correlations C^3. (a) Construction of the noise cross-correlations (red arrows) between stations A and B and all of the other stations S of the network. The blue stars represent distant sources of noise. (b) Construction of C^3 between A and B using the stations of the network as virtual sources (red stars).*

For a network of N stations, the C^3 function between two stations A and B is computed through the successive steps illustrated in Figure 9. Let a third station in the network be represented by S. The noise correlation is computed between A-S and B-S (Figure 9a, C^1). The noise correlation corresponds to the signals recorded at A and B, respectively, if a source was present at S. The receivers S have the role of virtual sources. The same operation is repeated for all of the stations S in the network. A time window in the later part of the noise correlations is selected (at twice the Rayleigh wave travel-time in Stehly et al. (2008)). Note that the codas for both the positive and negative parts of the noise correlation are selected. The correlations of the codas of the A-S and B-S noise correlations are computed for positive and negative times. The results are finally averaged for all of the virtual sources S of the network, to obtain the C^3 function between A and B (Figure 9b).

Note at this point that the geometry of the network controls the illumination of virtual sources for the C^3 computation. With this procedure, Stehly et al. (2008) showed that C^3

shows the ballistic Rayleigh waves of the Green's function, as demonstrated for actual coda-wave correlations (Campillo and Paul 2003). This demonstrates that the late part of the ambient-noise correlation function contains a physical signal, namely the scattered coda waves. This is important, as it opens the way for using this signal for further applications (see Section 7.2).

Froment et al. (2011) illustrated the concept of a virtual source used for C3 computation. They compared the time symmetry of both correlation functions (C^1 and C^3) for the particular case of the station pair of HAU-BOURR, as illustrated in Figure 10. In the C^3 correlation process, only the 55 network stations south of HAU-BOURR are considered (see Figure 10a). The noise records were filtered in the frequency band from 0.1 Hz to 0.2 Hz.

Figure 10. *(a) Map of Europe with orange stars corresponding to the 55 stations of the network used as virtual sources to construct the C^3 function between stations HAU and BOURR (red triangles). Note that all of the stations considered are located south of the HAU-BOURR path and opposite to the main source of noise located in the North Atlantic Ocean or on the northern European coast (gray zone). The black arrow indicates the main direction of ambient seismic noise in the vicinity of the station pair HAU-BOURR. (b) Noise correlation C^1 (orange curve) and C^3 (black curve) functions between stations HAU and BOURR for the geometry displayed in (a). Note the different vertical scales (left and right, respectively) for the two normalized correlation functions. (from Froment et al. 2011).*

This means that the theoretical C^3 virtual sources are located south of the station pair of interest and opposite to the incident-noise direction, as the main source of noise is located in the North Atlantic Ocean or on the northern European coast (e.g., Friedrich et al. 1998, Kedar et al. 2008, Landès et al. 2010, Stehly et al. 2006). Figure 10b shows the results of both the C^1 and C^3 correlation functions for this geometry. The time symmetry of both of the signals shows two opposite peaks of maximum amplitude, which reflect a main energy flux that propagates in opposite directions: from north to south for C^1, and from south to north for C^3. Note that the same convention is used for all of the correlation functions; i.e., the signal in negative (resp. positive) correlation times corresponds to waves propagating from north to south (resp. south to north). This observation indicates that the time symmetry of the two correlation functions is consistent with the location of their expected contributing source distributions (actual or virtual). However, the C^3 function has a better time symmetry than C^1. This indicates that the coda waves used to compute the C^3 function constitute a more isotropic

field than the ambient seismic noise. Back-scattered waves produce a north-to-south energy flux propagation and therefore contribute to a clear pulse in the negative correlation times.

Furthermore, Froment et al. (2011) also discussed the possibility of using the C^3 coda to reconstruct part of the Green's function. They computed a C^5 function, the **c**orrelation of the **c**oda of C^3, and they found that the Rayleigh wave is reconstructed. This shows that some coherent signal is still present in the coda of the C^3 function. This result supports the idea that the C^5 function can also be used in noise-based tomography or for monitoring techniques. However, the SNR in the C^5 function is smaller than that in the C^3 function, due to the reduction in the time-window length used for the computation of the correlation. This might limit the practical interest of this iterative correlation process.

The computation of the correlation of correlations is a way to control the illumination, and its isotropy, by using a network of stations as the part of the virtual sources. Furthermore, it allows for the separation of scattered and direct waves for the final correlation. This selection is obvious with the selection of an *ad-hoc* time window in noise correlations. From the opposite side, it is impossible to perform this separation with noise records in which direct and scattered waves from various sources are mixed. Although the coda of correlation takes advantage of the properties of multiply-scattered waves, it is also possible to compute the correlation of complete noise correlations, including the ballistic part (Froment et al., 2011). This is indeed of interest for long period waves for which the scattering is weak. The distribution of the stations, that play the role of virtual sources, is determinant in this case.

Ma and Beroza (2012) used the C^3 approach with data from stations that operate asynchronously, showing that it is practically possible to complement the virtual network with stations that were recording at different periods. Curtis and Halliday (2010) presented a series of integral relations essentially based on correlation or convolution of correlation functions that allowed for reconstructions of virtual seismograms from non-synchronous records; i.e., a record at a station that was not operating at the time of an event. Curtis et al. (2012) showed the application of these principles for an earthquake in New Zealand.

7- Applications

7-1 Surface-wave tomography

It is generally assumed that noise is related to surface activity, which ranges from human activity at high frequency to the forcing of the oceans and the atmosphere at low frequency.

As a consequence, the seismic noise observed at the surface has a strong component of surface waves, as has the Green's function between two surface points. The first attempts to extract the Green's function from coda or noise seismic records demonstrated the retrieval of surface waves (Campillo and Paul 2003, Shapiro et al. 2004). Numerous studies have confirmed that Rayleigh waves are easily retrieved from ambient-noise correlations. When surface waves are identified in ambient-noise correlations, the methods previously developed for earthquake records can be used to infer dispersion properties, and eventually tomographic images. Ambient-noise surface-wave measurements have been extensively used for tomography at the crustal and lithospheric scales (e.g.. Sabra et al. 2005b, Shapiro et al. 2005, Kang and Chin 2006, Yang et al. 2007, Lin et al. 2008, Nishida et al. 2008a, Yao et al. 2008, Zeng et al. 2008, Li et al. 2010, Saygin and Kennett 2010, Stehly et al. 2010, Ritzwoller et al. 2011, Poli et al. 2012c, Verbeke et al. 2012). Anisotropy has also been inferred (e.g., Huang et al. 2010, Ritzwoller et al. 2011). Harmon et al. (2007) and Yao et al. (2001) studied the oceanic lithosphere with ambient noise records from ocean bottom seismometers.

Ambient-noise tomography takes advantage of the dense networks by providing a large number of interstation measurements. This allows for improved resolution with respect to using distant earthquake records. This is particularly true for the short periods that are difficult to use when dealing with distant sources. With large dense networks, specific approaches can be applied. An example was presented by Ritzwoller et al. (2011) with eikonal tomography. This technique is based on direct measurement of the local velocity of a surface wave. This is achieved by use of the eikonal equation, with maps of travel-times measured and interpolated on a dense array. In the context of ambient-noise tomography, this operation can be performed with each station acting as a virtual source. When considering all possible virtual sources, a map of the seismic speed can be built, as a function of the azimuth of propagation. An application of these principles is illustrated in Figure 11, where the dense array of western USA is used to build a high-resolution map of Rayleigh wave speeds at 24 s, and a map of the amplitude of anisotropy and the direction of the fast axis (Ritzwoller et al. 2011).

Figure 11. *(a) The 24-s Rayleigh wave isotropic phase speed map taken from the ambient noise by averaging all of the local phase-speed measurements at each point on the map. (b) The amplitudes and fast directions of the 2c component of the 24-s Rayleigh wave phase velocities. The amplitudes of the anisotropy are given by the lengths of the bars, which point in the fast-axis direction, and the background is color-coded. At the 24-s period, the Rayleigh*

wave anisotropy reflects conditions in a mixture of the crust and the uppermost mantle (from Ritzwoller et al. 2011).

Ambient-noise surface-wave tomography has also been applied successfully at smaller scales, to volcanic structures (e.g., Brenguier et al. 2007), shallow surface layers (e.g., Picozzi et al. 2008) and landslides (e.g., Renalier et al. 2010). It is of note that Larose et al. (2005) reported a study of the lunar subsurface from the ambient noise recorded during the Apollo 17 mission.

7.2-Body waves

Although usually with weak amplitudes, body waves are present in the noise records. This was clearly shown with array analysis in recent studies (e.g., Gerstoft et al. 2008, who identified mantle and core phases), and body waves have been used to map the regions were noise is produced at a global scale (e.g., Landès et al. 2010).

There is therefore substantial hope of extracting the body-wave part of the Green's function, albeit with a lower SNR than for the dominant surface waves. Actually, body waves have indeed been reported from short-distance range correlations. Roux (2005a) identified direct P-waves from noise correlation, using data from a small array in California, USA. Their noise-derived P-waves were linearly polarized, and with an apparent velocity compatible with a known velocity model of the area. Several studies have claimed that there are reflected phases in ambient-noise autocorrelations and cross-correlations. Draganov et al. (2009) used data from oil exploration surveys to extract reflected P-waves from shallow interfaces. Their observations appeared to be in good agreement with the active source reflection response measured in the same area. Tibuleac and von Seggern (2012) reported that a vertical Moho reflection can be identified in autocorrelations in Nevada, USA. Ito and Shiomi (2012) used ambient noise to extract reflections associated with a subducting slab beneath Japan.

Zhan et al. (2010) identified S reflected phases from the Moho interface at the critical distance in two shield areas. Poli et al. (2012a) built a short-period seismic section across Finland from ambient-noise correlation. They used the continuous records of 42 temporary broadband three-component stations located in the northern part of the Fenno-Scandian region (Figure 12a). Here, they identify high-frequency body waves (0.5-2.0 Hz) emerging from noise correlations for inter-station distances up to 550 km. The comparisons of the noise correlations with earthquake data confirmed that the observed waves can be interpreted as P-

waves and S-waves that are reflected from the Moho. As the crustal model of the area is well known, the noise correlations can be compared with synthetic seismograms. Figure 12 shows an example of such a comparison for two different components of motion: it indicates that the travel-times of all of the observed phases are in excellent agreement. Poli et al. (2012) also performed a polarization analysis that confirmed that reflected body waves are positively extracted from ambient noise.

Figure 12. *(a) Map of the stations of the LAPNet experiment in Finland. (b) ZZ and (d) RR cross-correlations plotted as functions of inter-station distances. (c) The vertical component (Z) of synthetic seismograms for a vertical point force at the surface. (e) The radial component (R) of synthetic seismograms for a horizontal point force at the surface. All of the signals were filtered between 0.5 Hz and 1.0 Hz (modified from Poli et al. 2012a).*

A step further is to demonstrate that deep seismic phases can be retrieved from ambient noise. Poli et al. (2012b) used noise in the microseism band to retrieve P-waves reflected at the top (*ca*. 410 km deep) and at the bottom (*ca*. 660 km deep) of the transition zone. Figure 13 shows the stacked correlations for the pairs of the LAPNet array (see Figure 12a), as compared with the preferred velocity model. This demonstration that deep interfaces can be imaged with ambient noise at the surface confirms that the ambient noise in the microseism band consists partly of body-waves propagating at the global scale and illuminating the deep interior. This opens the way for the use of ambient-noise correlations to image the deep Earth using body waves. Deep core reflexions were reported from correlations at regional distances by Lin et al. (2013). Nishida (2013) and Boué et al. (2013) presented global sections of cross-correlations indicating that most of the deep phases could be extracted from ambient noise.

Figure 13. *(a) Comparison of stacked cross-correlation (data) with synthetic traces computed for the global model AK135, and for the final preferred model beneath Finland depicted in (b). The map of the stations used in this study is shown in Figure 12a.*

7.3-Monitoring

Monitoring of slight changes in velocity in the Earth can be performed with active sources (e.g., Reasenberg and Aki 1973, Niu et al. 2008) or with repeating earthquakes (Poupinet et al. 1984, Ratdomopurbo and Poupinet 1995).

The possibility of using the ambient noise to perform repeated measurements of speeds between fixed stations is appealing. In the previous sections we discussed the convergence of the cross-correlation towards the Green's function for continuous records of ambient noise of finite duration. Careful attention must be paid to the quality of the reconstruction and to the possible bias associated with the angular distribution of the incoming noise energy. With these precautions, it is possible to repeat the processing at different dates, and therefore to track temporal changes in the medium.

The first requirement is to study the stability of the measurements and to detect possible instrumental errors when using cross-correlations. As the unbiased physical signals have to be time symmetric, the comparison of the arrival times in the positive and negative correlation times of the Rayleigh and Love waves allows the separation of time shifts associated with any form of physical change in the medium, so those resulting from clock drift or other instrumental errors, and those due to changes in the localization of the noise sources (e.g., Stehly et al. 2007). Physical changes of the medium speed result in delays of the same amplitude for positive and negative times. Instrumental changes produce a global shift of the correlation with opposite time-delays. Bias due to nonisotropic illumination (see section 5) is associated with different noise sources, and is not likely to be equal for positive and negative times. These arguments allow for the detection of instrumental errors and for the correcting for them.

Measuring very small relative velocity changes requires the evaluation of delays between traces. Under the assumption of a global change, these delays increase with the travel times, making the detection much easier for large lapse times. For this reason, it is often more difficult to detect small material changes with direct waves than with waves that have sampled the medium for much longer times, as is the case with coda waves.

In section 6.2, we discussed the properties of the C^3 function. The convergence of C^3 towards the Green's function demonstrates that the late part of the correlation functions contains scattered waves. Schönfelder and Wegler (2006) found that the envelope of the correlation of noise is similar for the different components of the correlation tensor, as expected for coda waves, and that this envelope can be modeled with a diffusion equation. Indeed, these arguments do not demonstrate that the entire coda is perfectly reconstructed. This is not a requirement to use the correlations for monitoring changes in velocity. With laboratory ultrasound experiments, Hadziioannou et al. (2009) showed that passive monitoring can be successful without complete reconstruction of the Green's function from cross-correlations. While the noise source is variable, it is observed that the late part of the

noise correlation function is very stable and allows for the monitoring of slight changes in velocity.

7.3.1-Velocity change detection and measurement

The delay dt measured before and after a global change in a medium increases linearly with lapsed time t, according to the simple relationship:

$$\frac{dt}{t} = -\frac{dV}{V} \qquad (66),$$

where dV/V is the relative velocity change. This is the basis for very precise measurements of velocity change with coda waves. Poupinet et al. (1984) and Snieder et al. (2002) proposed to measure dt in moving windows along seismograms, to evaluate dV/V through linear regression (moving-window cross-spectral analysis; MWSPA). Alternatively, the stretching technique consists of optimization of a stretching parameter ε (e.g., Lobkis and Weaver 2003, Sens-Schönfelder and Wegler 2006). The effect of a global small velocity change is to deform the trace by changing the time t by t' = t (1-ε_0). The strategy is to interpolate the coda at times t (1 − ε) with various stretching factors ε.

The actual relative velocity change is the stretching factor ε_0 = dV/V that maximizes the cross-correlation coefficient between the traces that is acquired before and after the change. Hadziioannou et al. (2009) showed that the stretching technique is more adapted to data with low SNRs in the presence of an actual global velocity change.

Repeated delay measurements have been applied to autocorrelations and cross-correlations, which have demonstrated the possibility to observe relative changes in speed of the medium as small as 10^{-4}. The evaluation of uncertainties is an important issue. Clarke et al. (2010) analyzed the uncertainties of MWSPA in the context of ambient-noise monitoring of a volcano. They concluded that the formal error deduced from the linear regression in MWSPA underestimated the observed fluctuations of velocity when a small amount of noise was added to the correlations. With the stretching method, the dependence of the uncertainty on the correlation coefficient between the traces and the parameters of measure (bandwidth, time window) was given by Weaver et al. (2011).

7.3.2-Observations

The velocity changes observed with ambient noise are likely to be of various origins. Schönfelder and Wegler (2006) studied the autocorrelations of noise records on a volcano, and they detected a seasonal velocity change that they interpreted as being related to the variations of the water-table depth. Meier et al. (2010) attributed the seasonal changes of velocity observed in the Los Angeles basin to a thermo-elastic effect. Brenguier et al. (2008a) used long time series and detected a velocity change that was precursory to volcanic eruptions of the Piton de la Fournaise volcano. This was interpreted as the effect of the inflation of the edifice prior to the eruption. Mainsant et al. (2012) also used ambient noise to detect a drop in velocity prior to a landslide.

Recently, several studies have shown the detection of velocity changes associated with the activity of fault systems, earthquakes and transient creep, with correlations of ambient noise. Wegler and Schönfelder (2007) detected a change in velocity after the Mw 6.6 mid-Niigata earthquake in Japan. Brenguier et al. (2008b) observed velocity drops associated with two earthquakes in central California, USA (Figure 14).

Figure 14. *Seismic velocity changes, surface displacements from GPS, and tremor activity near Parkfield. The red curve represents the post-seismic fault-parallel displacements along the San Andreas fault, as measured by GPS at a local station. The tremor rates are averaged over a centered 30-day-length moving time window (from Brenguier et al. 2008b).*

More recently, Hadziioannou et al. (2011) used the adaptive filtering approach of Baig et al. (2009) to improve the time resolution of the monitoring, and they concluded that the velocity drop associated with the Parkfield earthquake is co-seismic with a precision of one day. Considering the apparent similarity of the temporal evolution of the velocity change, GPS position, and tremor activity at depth, Brenguier et al. (2008b) proposed that the velocity change is not only related to the well-documented nonlinear response of the shallow layers to strong motion. Wegler et al. (2009) reached a similar conclusion on the existence of a change at depth for the sudden drop in velocity observed after the 2004 Mw 6.6 mid-Niigata earthquake in Japan. Chen et al. (2010) and Froment et al. (2013) studied the case of the 2008 Mw 7.9 Wenchuan earthquake, and they also found a velocity drop associated with the earthquake. They used broadband ambient-noise records and preformed the measurements in the two separate period bands of 1 s to 3 s and 12 s to 20 s. The amplitude of the velocity drop was larger for the long-period band. As the measurements are performed with coda waves, they have the depth sensitivity of the predominant surface waves. The results therefore

suggest that the change occurs also at depth and affects the middle crust. Furthermore, whether the temporal velocity change is related to deformation at depth can be investigated in the case of slow-slip events that produce significant deformation at depth without strong ground motion at the surface. Rivet et al (2011) found a transient change in the velocity at depth associated with a large (Mw 7.5) slow-slip event on the Mexican subduction.

Despite promising evidence for the feasibility of monitoring deformation at depth with seismic ambient noise, it is noticeable that the origin of the changes can be obscured by the coincidence of signals of tectonic and hydrological origins (e.g., Yu and Hung 2012, Froment et al. 2013).

8-Conclusions

Ambient-noise correlation is emerging as a new tool in seismic data processing. It is complementary to the traditional use of earthquake or active source records. The correlation of ambient-noise records at distant points can be regarded, under certain conditions, as the virtual seismogram recorded at one point if a source was acting at the other.

We have shown physical representations that allow the reader to have an intuitive understanding of the method. The emergence of the Green's function in cross-correlation is the expression of the fundamental properties of wave fields. This is illustrated by the analogy with time-reversal mirrors that have shown the reconstruction of converging and diverging Green's functions in laboratory experiments. We have also presented a geometrical interpretation that shows that source averaging tends to select the contribution of sources located in the end-fire lobes. We have presented mathematical results that show that the construction of virtual seismograms is rigorous, and that the complete deterministic response of the Earth can be extracted from the records at distant points.

In practice, the ambient noise is produced by sources that are unevenly distributed. In general, this results in incomplete or improper reconstruction. We have analyzed the impact of a nonisotropic distribution of incident noise intensity on the travel-times measured on correlations. There is bias, but it is predictable accurately, meaning that corrections can be applied when necessary. With realistic distributions, the method is robust and the bias in the travel-time is acceptable for most imaging applications.

The presence of scattering due to the heterogeneous nature of the Earth results in complexity of the seismic wave field. As this complexity tends to spread the wave energy over a wide range of directions and to enhance the conversion between the types of waves, it

also has a positive role for the correlation of noise. For long lapse times, the field becomes diffuse, and has in itself the properties sufficient to obtain the Green's function by correlation. Theoretically, a single source would be sufficient to produce an equipartioned field, with its two-point average correlation being the Green's function. This can be understood by considering the scatterers as secondary sources that are uniformly distributed in the medium. With actual normalized noise records, the ballistic waves produced by noise sources are supplemented by the scattered waves of the Earth heterogeneity.

The relatively easy extraction of surface waves by the correlation of noise records has made it possible to apply ambient surface tomography in different places around the world. With this technique, high-resolution crustal models have been proposed, including for shear-wave velocity, anisotropy and attenuation. Applications have been realized at different scales. Based on the general mathematical properties discussed in section 4, and the observation of a teleseismic body-wave component in the noise records, the reconstruction of body waves is expected and has been confirmed by recent studies. This opens the way to the generalization of ambient-noise tomography to all types of waves, including deep phases.

As ambient-noise cross-correlation can be repeated at different dates, these cross-correlations can be used to monitor slight changes in the elastic properties of the crust. The late part of correlations, corresponding to the coda waves, computed at different dates are very stable and allow for the measuring of slight relative changes of seismic speeds, as small as 10^{-4}. Changes in seismic velocity have been observed after large earthquakes in several studies, including for slow-slip events. Velocity drops have been proposed to be precursory to volcanic eruptions and landslides.

The exploitation of ambient seismic noise is an emerging field. The huge datasets produced nowadays by dense permanent and temporary networks offer new opportunities for the development of innovative techniques to construct virtual seismograms that correspond to paths in regions of the planet that are poorly covered. Ambient-noise analysis will continue to provide new insights into the structure of the Earth and into its continuous evolution.

9-References

Abramowitz, M. and I. A. Stegun (1972). Handbook of mathematical functions, Dover Publications Inc., New York.

Aki, K. (1957), Space and time spectra of stationary stochastic waves with special reference to microtremors, Bull. Earthq. Res. Inst. 35, 415–456.

Ardhuin, F., E. Stutzmann, M. Schimmel, and A. Mangeney (2011), Ocean wave sources of seismic noise, J. Geophys. Res., 116, C09004, doi:10.1029/2011JC006952.

Baig, A. M., M. Campillo, and F. Brenguier (2009), Denoising seismic noise cross correlations, J. Geophys. Res., 114, B08310, doi:10.1029/2008JB006085.

Bensen, G.D., Ritzwoller, M.H., Barmin, M.P., Levshin, A.L., Lin, F., Moschetti, M.P., Shapiro, N.M., Yang, Y., 2007. Processing seismic ambient noise data to obtain reliable broad-band surface wave dispersion measurements. Geophys. J. Int. 169, 1239–1260.

Bonnefoy-Claudet, S., F. Cotton, and P.-Y. Bard. (2006) The nature of noisewavefield and its applications for site effect studies—A literature review, Earth Sci. Rev. 79, 205–227.

Boué, P., P. Poli, M. Campillo, H. Pedersen, X. Briand, P. Roux. (2013) Teleseismic correlations of ambient seismic noise for deep global imaging of the Earth, in press Geophys. J. Int.

Brenguier, F., N. M. Shapiro, M. Campillo, A. Nercessian, and V.Ferrazzini (2007), 3-D surface wave tomography of the Piton de la Fournaise volcano using seismic noise correlations, Geophys. Res. Lett., 34, L02305, doi:10.1029/2006GL028586

Brenguier, F., Campillo, M., Hadziioannou, C., Shapiro, N., Nadeau, R. M., and Larose, E. (2008b). Postseismic relaxation along the San Andreas fault at Parkfield from continuous seismological observations. Science, 321(5895) :1478–1481.

Brenguier, F., N. M. Shapiro, M. Campillo, V. Ferrazzini, Z. Duputel, O. Coutant, and A. Nercessian (2008a), Towards forecasting volcanic eruptions using seismic noise, Nat. Geosci., 1, 126–130, doi:10.1038/ngeo104.

Campillo, M. and Paul, A. (2003), Long-range correlations in the seismic coda, Science 299, 547–549.

Campillo, M. (2006) Phase and Correlation in 'Random' Seismic Fields and the Reconstruction of the Green Function (2006) Pure and Applied Geophysics 163, 475-502.

Campillo, M. and L. Margerin (2010) Mesoscopic seismic waves in New Directions in Linear Acoustics and Vibration in Quantum Chaos, Random Matrix Theory and Complexity M. Wright and R. Weaver Eds, Cambridge University Press.

Chen, J., B. Froment, Q.Y. Liu and M. Campillo (2010), Distribution of seismic wave speed changes associated with the 12 May 2008 Mw 7.9 Wenchuan earthquake, Geophys. Res. Letters, VOL. 37, L18302, doi:10.1029/2010GL044582.

Claerbout, J., 1968, Synthesis of a layered medium from its acoustic transmission response: Geophysics, 264-269.

Clarke, D., L. Zaccarelli, N. M. Shapiro and F. Brenguier (2011) Assessment of resolution and accuracy of the Moving Window Cross Spectral technique for monitoring crustal temporal variations using ambient seismic noise, Geophys. J. Int. Article first published online: 21 JUN 2011 | DOI: 10.1111/j.1365-246X.2011.05074.x.

Courtland, R. (2008), Harnessing the hum, Nature, 453, 146–148, doi:10.1038/453146a.

Cupillard, P., Capdeville, Y., 2010. On the amplitude of surface waves obtained by noise correlation and the capability to recover the attenuation: a numerical approach. Geophys. J. Int. 181, 1687–1700.

Cupillard, P., Stelhy, L. & Romanowicz, B., 2011. The one-bit noise correlation: a theory based on the concepts of coherent and incoherent noise. Geophys. J. Int., 184, 1397–1414.

Curtis, A., P. Gerstoft, H. Sato, R. Snieder, and K. Wapenaar, 2006, Seismic interferometry–-turning noise into signal. The Leading Edge, 25, 1082–1092, doi: 10.1190/1.2349814.

Curtis, A. and D. Halliday, 2010. Source-receiver wave field interferometry. Physical Review E, Vol.81, No.4, pp. 046601-1 - 046601-10. doi: 10.1103/PhysRevE.81.046601

Curtis, A., Y. Behr, E. Entwistle, E. Galetti, J. Townend, S. Bannister, 2012. The benefit of hindsight in observational science: retrospective seismological observations. Earth and Planetary Science Letters,vol. 345-348, pp. 212-220

Colin de Verdière, Y., 2009. Semiclassical analysis and passive imaging. Nonlinearity 22, R45–R75.

Colin de Verdière, Y., 2011. A semi-classical calculus of the correlations, Compte Rend. Geosc., 343, 496–501.

Derode A., E. Larose, M. Campillo and M. Fink (2003), How to estimate the Green's function of a heterogeneous medium between two passive sensors ? Application to acoustic waves. Applied Physics Letters, 83 (15), 3054-3056. Article.PDF

Derode A., E. Larose, M. Tanter, J. de Rosny, A. Tourin, M. Campillo and M. Fink (2003), Recovering the Green's function from field-field correlations in an open scattering medium, Journal of the Acoustical Society of America, 113, 2973-2976.

Duvall, T.L. Jr., S.M. Jefferies, J.W. Harvey, and M.A. Pomerantz. 1993. Time-distance helioseismology. Nature, 362 (6419), 430.

Draganov, D., Campman, X., Thorbecke, J., Verdel, A. & Wapenaar, K., 2009, Reflection images from ambient seismic noise. Geophysics, 74, 63–67.

Fink, M. (1992), Time reversal of ultrasonic fields- Part I: Basic principles, IEEE Trans. Ultrason., Ferroelec., Freq. Contr. 39(5), 555–566.

Friederich, A., Kruger, F., and Klinge, K. (1998), Ocean-generated microseismic noise located with the GRFO array, J. Seismol. 2, 47–64.

Froment B. , Campillo M. , Roux P., Gouedard P. , Verdel A., Weaver R.L. (2010) Estimation of the effect of nonisotropically distributed energy on the apparent arrival time in correlations GEOPHYSICS 75, SA85-SA93 .

Froment, B., M. Campillo and P. Roux (2011), Reconstructing the Green's function through iteration of correlations, Comptes Rendus Geoscience, Volume : 343, Issue : 8-9, Pages : 623-632, DOI : 10.1016/j.crte.2011.03.001

Froment, B., M. Campillo, J.H. Chen and Q.Y. Liu (2013) Deformation at depth associated with the May 12, 2008 Mw 7.9 Wenchuan earthquake from seismic ambient noise monitoring. Geophysical Research Letters, Volume 40 78–82, doi:10.1029/2012GL053995

Fukao, Y., K. Nishida, and N. Kobayashi (2010), Seafloor topography, ocean infragravity waves, and background Love and Rayleigh waves, J. Geophys. Res., 115, B04302, doi:10.1029/2009JB006678.

Gallot, T., S. Catheline, P. Roux and M. campillo (2012) A passive inverse filter for Green's function retrieval JOURNAL OF THE ACOUSTICAL SOCIETY OF AMERICA Volume: 131 Issue: 1 Pages: EL21-EL27 DOI: 10.1121/1.3665397

Garnier, J., Papanicolaou, G., 2009. Passive sensor imaging using crosscorrelations of noisy signals in a scattering medium. SIAM J. Imaging Sci. 2 (2), 396–437.

Gerstoft, P., Shearer, P.M., Harmon, N. & Zhang, J., 2008. Global P, PP, and PKP wave microseisms observed from distant storms, Geophys. Res. Lett., 35, L23307, doi:10.1029/2008GL036111.

Godin, O.A. (2007) Emergence of the acoustic Green's function from thermal noise. J. Acoust. Soc. Am. 121, EL96

Gouédard, P., L. Stehly, F. Brenguier, M. Campillo, Y. Colin de Verdière, E. Larose, L. Margerin, P. Roux, F. J. Sanchez-Sesma, N. M. Shapiro and R. L. Weaver: *Cross-correlation of random fields: mathematical approach and applications*, Geophysical Prospecting 56, 375-393 (2008).

Gouédard, P., P. Roux, M. Campillo and A. Verdel (2008) Convergence of the two-points correlation function toward the Green's function in the context of a prospecting dataset.GEOPHYSICS Volume: 73 Issue: 6 Pages: V47-V53

Gutenberg, B. (1924), Die seismischen Bodenunruhe, Samml. Geophysikalischer Schr., 3, 1–69.

Gutenberg, B., (1958) Microseisms. Advances in Geophysics 5, 53–92.

Hadziioannou, C., E. Larose, O. Coutant, P. Roux, and M. Campillo (2009), Stability of monitoring weak changes in multiply scattering media with ambient noise correlation: Laboratory experiments, J. Acoust. Soc. Am., 125(6), 3688–3695.

Hadziioannou, C., E. Larose, A. Baig, P. Roux, and M. Campillo (2011), Improving temporal resolution in ambient noise monitoring of seismic wave speed, J. Geophys. Res., 116, B07304, doi:10.1029/2011JB008200.

Hanasoge, S.M. (2013) The influence of noise source on cross-correlation amplitudes Geophys. J. Int. 192, 295-309.

Harmon, N., D. Forsyth, and S. Webb (2007) Using Ambient Seismic Noise to Determine Short Period Phase Velocities and Shallow Shear Velocities in Young Oceanic Lithosphere. Bulletin of the Seismological Society of America, 97, (6), 2009-2023.

Haubrich, R. A. Munk, W. H. Snodgrass, F. E. (1963). Comparative spectra of microseisms and swell, Bull. Seism. Soc. Am. 53, 27- 37.

Hennino, R., N. Trégourès, N. Shapiro, L. Margerin, M. Campillo, B. van Tiggelen and R.L. Weaver (2001) Observation of Equipartition of seismic waves in Mexico Physical Review Letters 86-15, 3447-3450.

Hillers, G., N. Graham, M. Campillo, S. Kedar, M. Landès, and N. Shapiro (2012), Global oceanic microseism sources as seen by seismic arrays and predicted by wave action models, Geochem. Geophys. Geosyst., 13, Q01021, doi:10.1029/ 2011GC003875.

Huang, H., Yao, H., van der Hilst, R.D., 2010. Radial anisotropy in the crust of SE Tibet and SW China from ambient noise interferometry, Geophys. Res. Lett., doi:10.1029/2010GL044981

Ito, Y., *and* K. Shiomi *(*2012*),* Seismic scatterers within subducting slab revealed from ambient noise autocorrelation*,* Geophys. Res. Lett*.,* 39*, L19303, doi:*10.1029/2012GL053321.

Kang, T.S. & Shin, J.S., 2006. Surface-wave tomography from ambient seismic noise of accelerograph networks in southern Korea, Geophys. Res. Lett., 33, 1–5, doi:10.1029/2006GL027044.

Kedar, S., M. Longuet-Higgins, F. Webb, N. Graham, R. Clayton, and C. Jones (2008), The origin of deep ocean microseisms in the North Atlantic Ocean, Proc. R. Soc. A, 464, 777–793, doi:10.1098/rspa.2007.0277.

Kobayashi, N., and K. Nishida (1998), Continuous excitation of planetary free oscillations by atmospheric disturbances, Nature, 395, 357–360, doi:10.1038/26427.

Kurrle, D., and R. Widmer-Schnidrig (2008), The horizontal hum of the Earth: A global background of spheroidal and toroidal modes, Geophys. Res. Lett., 35, L06304, doi:10.1029/2007GL033125.

Landès, M., F. Hubans, N. M. Shapiro, A. Paul, and M. Campillo (2010), Origin of deep ocean microseisms by using teleseismic body waves, J. Geophys. Res., 115, B05302, doi:10.1029/2009JB006918.

Larose, E., L. Margerin, B.A. van Tiggelen and M. Campillo (2004) Observation of Weak Localization of Seismic Waves *Physical Review Letters* 94-4, 10.1103/ Phys Rev Lett.93.048501 (1-4)

Larose, E., A. Khan, Y. Nakamura, and M. Campillo (2005) Lunar subsurface investigated from correlation of seismic noise, Geophys. Res. Let. doi: 10.1029/2005GL023518 (2005).

Larose, E., J. De Rosny, L. Margerin, D. Anache, P. Gouédard, M. Campillo, and B. Van Tiggelen (2006) *Observation of multiple scattering of kHz vibrations in a concrete structure and application to monitoring weak change,*Phys. Rev. E **73** 016609.

Larose, E., P. Roux, M. Campillo, A. Derode: Fluctuations of correlations and Green's function reconstruction: role of scattering, J. Appl. Phys. 103, 114907 (2008)

Larose, E., L. Margerin, A. Derode, B. van Tiggelen, M. Campillo, N. Shapiro, A. Paul, L. Stehly, M Tanter (2006): *Correlation of random wave fields: an interdisciplinary review,* Geophysics 71, NO. 4. SI11–SI21, 8 FIGS.10.1190/1.2213356.

Lawrence, J. F., G. A. Prieto, (2011). Attenuation tomography in the western United States from ambient seismic noise. J. Geophys. Res. 116, B06302, doi:10.1029/ 2010JB007836.

Li, H., Bernardi, F.,and Michelini, A., 2010. Surface wave dispersion measurements from ambient seismic noise analysis in Italy, Geophys. J. Int., 180, 1242–1252.

Lin, F.C., Ritzwoller, M.H., Snieder, R., 2009. Eikonal tomography: surface wave tomography by phase front tracking across a regional broad-band seismic array. Geophys. J. Int. 177, 1091–1110.

Lin, F.C., Ritzwoller, M.H., Yang, Y., Moschetti, M.P., Fouch, M.J., 2011a.
Complex and variable crust and uppermost mantle seismic anisotropy in the western US. Nature Geosci. 4 (1), 55–61.

Lin, F.-C., V. C. Tsai, B. Schmandt, Z. Duputel, *and* Z. Zhan *(*2013*),* Extracting seismic core phases with array interferometry, Geophys. Res. Lett., 40, 1049–1053, *doi:*10.1002/grl.50237.

Lobkis, O. I. and R. L. Weaver (2001). On the emergence of the Green's function in the correlations of a diffuse field, J. Acoust. Soc. Am 110, 3011-3017.

Lobkis, O. and Weaver, R. (2003). Coda-Wave Interferometry in Finite Solids : Recovery of P-to-S Conversion Rates in an Elastodynamic Billiard. Phys. Rev. Lett., 90(25) :254302. 21, 40, 43, 44, 63, 81, 97, 113, 114

Longuet-Higgins, M. S. (1950). A theory of the origin of microseisms, Philos. Trans. R. Soc. London 243, 1-35.

Mainsant, G, E. Larose, C. Brönnimann, D. Jongmans, C. Michoud, M. Jaboyedoff (2012) Ambient seismic noise monitoring of a clay landslide: Toward failure prediction, J. Geophys. Res., 117, *F01030, doi:*10.1029/2011JF002159.

Ma, S. and G. C. Beroza (2012), Ambient-field Green's functions from asynchronous seismic observations, Geophys. Res. Lett., 39, L06301, doi:10.1029/2011GL050755.

Margerin L, Campillo M, Van Tiggelen BA, Hennino, R. Energy partition of seismic coda waves in layered media: theory and application to Pinyon Flats Observatory GEOPHYSICAL JOURNAL INTERNATIONAL Volume: 177 Issue: 2 Pages: 571-585 2009

Margerin, L. and H. Sato, Reconstruction of multiply-scattered arrivals from the cross-correlation of waves excited by random noise sources in a heterogeneous dissipative medium, Wave Motion, 48, 146-160, 2011.

Meier U., Brenguier F., Shapiro N., 2010. Detecting seasonal variations in seismic velocities within Los Angeles basin from correlations of ambient seismic noise, Geophys. J. Int., 181, 985-996, doi: 10.1111/j.1365-246X.2010.04550.x

Miche, A. (1944), Mouvements ondulatoires de la mer en profondeur croissante ou décroissante: Première partie. Mouvements ondulatoires périodiques et cylindriques en profondeur constante, Ann. Ponts Chaussées, 114, 42–78.

Nakahara, H., 2006. A systematic study of the theoretical relations between spatial correlations and Green's function in one-, two- and three-dimensional random scalar wavefields, Geophys. J. Int., 167, 1097–1105.

Nishida, K., H. Kawakatsu, and K. Obara (2008a), Three-dimensional crustal S-wave velocity structure in Japan using microseismic data recorded by Hi-net tiltmeters, J. Geophys. Res.,

doi:10.102.

Nishida, K., H. Kawakatsu, Y. Fukao, and K. Obara (2008b) Background Love and Rayleigh waves simultaneously generated at the Pacific Ocean floors, Geophys. Res. Lett., 35, L16307, doi:10.102.

Nishida, K., J.P. Montagner and H. Kawakatsu, Global Surface Wave Tomography Using Seismic Hum, Science, 326, 5942, 112--112, 2009.

Nishida, K. (2013) Global propagation of body waves revealed by cross-correlation analysis of seismic hum in press Geophys. Res. Lett.,

Niu F, Silver PG, Daley TM, Cheng X, Majer EL (2008) Preseismic velocity changes observed from active source monitoring at the Parkfield SAFOD drill site. Nature. 454, doi:10.1038/nature07111.

Ohmi, S., K. Hirahara, H. Wada, and K. Ito (2008), Temporal variations of crustal structure in the source region of the 2007 Noto Hanto earthquake, central Japan, with Passive Image Interferometry, Earth Planets Space, 60, 1069–1074.

Paul, A., M. Campillo, L. Margerin, E. Larose and A. Derode (2005) Empirical synthesis of time-asymmetrical Green function from the correlation of coda waves Journal of Geophysical Research, 110, doi:10.1039/2004JB003521.

Peterson, J. (1993), Observations and modeling of seismic background noise, U.S. Geol. Surv. Open File Rep., 93-322, 1.

Picozzi, M.; Parolai, S.; Bindi, D.; Strollo, A. (2008): Characterization of shallow geology by high-frequency seismic noise tomography, Geophysical Journal International, 176, 1, 164-174.

Poli P., H. A. Pedersen, M. Campillo and the POLENET/LAPNET Working Group (2012a), Emergence of body waves from cross-correlation of short period seismic noise Geophys. J. Int.188, 549–558 doi : 10.1111/j.1365-246X.2011.05271.x.

Poli, P, M. Campillo, H. Pedersen and the Lapnet Working Group (2012c) Body wave imaging of the Earth's mantle discontinuities from ambient seismic noise, Science 338 p 1063-1066.

Poli, P. , H. A. Pedersen, M. Campillo, and the POLENET/LAPNET Working Group,(2012b) Noise directivity and group velocity tomography in a region with small velocity contrasts : the northern Baltic Shield. In press Geophysical Journal International.

Poupinet, G., Ellsworth,W. L. & Frechet, J. (1984) Monitoring velocity variations in the crust usingearthquake doublets: An application to the Calaveras Fault, California. J. Geophys. Res. 89,5719–5731.

Prieto, G.A., Lawrence, J.F., Beroza, G.C., 2009. Anelastic Earth structure from the coherency of the ambient seismic field. J. Geophys. Res. 114, B07303.

Prieto,G.A., Denolle, M., Lawrence, J.F. & Beroza, G.C., 2011. On the amplitude information carried by ambient seismic field, Compte Rend. Geosc., 343, 600–614.

Ratdomopurbo, A. & Poupinet, G. Monitoring a temporal change of seismic velocity in a volcano: Application to the 1992 eruption of Mt. Merapi (Indonesia). Geophys. Res. Lett. 22, 775–778 (1995).

Reasenberg, P., and K. Aki (1974), A precise, continuous measurement of seismic velocity for monitoring in situ stress, J. Geophys. Res., 79(2), 399–406.

Renalier, F., D. Jongmans, M. Campillo, and P. ‐ Y. Bard (2010), Shear wave velocity imaging of the Avignonet landslide (France) using ambient noise cross correlation, J. Geophys. Res., 115, F03032, doi:10.1029/2009JF001538.

Rhie, J., and B. Romanowicz (2004), Excitation of Earth's continuous free oscillations by atmosphere-ocean-seafloor couplinng, Nature, 431, 552–554.

Rivet, D., M. Campillo, N. M. Shapiro, V. Cruz-Atienza, Mathilde Radiguet,Nathalie Cotte, Vladimir Kostoglodov (2011), Seismic evidence of nonlinear crustal deformation during a

large slow slip event in Mexico Geophysical Research Letters, Volume : 38, Article Number : L08308 DOI : 10.1029/2011GL047151 Published : APR 28 2011.

Ritzwoller, M.H., F.C. Lin, and W. Shen, Ambient noise tomography with a large seismic array, Compte Rendus Geoscience, 13 pages, doi:10.1016/j.crte.2011.03.007, 2011.

Roux P. and W.A. Kupermann (2004) Extraction of coherent wavefronts from ocean ambient noise, J. Acoust. Soc. Am., 116 (4), pp. 1995-2003.

Roux, P., K. G. Sabra, P. Gerstoft, W. A. Kuperman, and M. C. Fehler (2005), P-waves from cross-correlation of seismic noise, Geophys. Res. Lett., 32, L19303, doi:10.1029/ 2005GL023803.

Roux, P., K. G. Sabra, W. A. Kuperman and A. Roux (2005). Ambient noise cross correlation in free space: Theoretical approach, J. Acoust. Soc. Am. 117, 79-84.

Ryzhik, L. V., G. C. Papanicolau and J. B. Keller (1996). Transport equations for elastic and other waves in random media, Wave Motion 24, 327-370.

Sabra, K. G., P. Gerstoft, P. Roux, W. A. Kuperman and M. C. Fehler (2005a). Extracting time-domain Green's function estimates from ambient seismic noise, Geophys. Res. Lett. 32, L03310, doi:10.1029/2004GL021862.

Sabra, K. G., P. Gerstoft, P. Roux, W. A. Kuperman, and M. C. Fehler (2005b), Surface wave tomography from microseisms in southern California, Geophys. Res. Lett., 32, L14311, doi:10.1029/2005GL023155.

Sánchez-Sesma F J and Campillo M. (2006). Retrieval of the Green function from cross-correlation: The canonical elastic problem. Bull. Seism. Soc. Am.96: 1182-1191.

Sànchez-Sesma, F.J., J.A. Pérez-Ruiz, M. Campillo,and F. Luzòn (2006) Elastodynamic 2D Green function retrieval from cross-correlation: Canonical inclusion problem Geophysical Research Letters, VOL. 33, L13305, doi:10.1029/2006GL026454

Sato, H.,_Retrieval of Green's function having coda from the cross-correlation function in a scattering medium illuminated by surrounding noise sources on the basis of the first order Born approximation, Geophys. J. Int., 179, 408-412, 2009.

Sato, H.,_Green's function retrieval from the CCF of coda waves in a scattering medium, Geophys. J. Int., 179, 1580–1583, 2009.

Sato, H., M.C. Fehler and T. Maeda (2012) Seismic wave propagation and scattering the heterogeneous Earth, (second edition) Springer editor

Saygin, E.&Kennett, B.L.N., 2010. Ambient seismic noise tomography of Australian continent, Tectonophysics, 481, 116–125.

Schimmel, M., E. Stutzmann and J. Gallart Using instantaneous phase coherence for signal extraction from ambient noise data at a local to a global scale Geophys. J. Int. (2011) 184, 494–506doi: 10.1111/j.1365-246X.2010.04861.

Schuster, G.T. (2006) Seismic interferometry, Cambridge University Press, Cambridge, UK, 2009.

Sens-Schönfelder, C. &Wegler, U. (2006). Passive image interferometry and seasonal variations of seismicvelocities at Merapi Volcano, Indonesia. Geophys. Res. Lett. 33, L21302

Shapiro, N. M., and M. Campillo (2004), Emergence of broadband Rayleigh waves from correlations of the seismic ambient noise, Geophys. Res. Lett., 31, L07614, doi:10.1029/ 2004GL019491.

Shapiro, N. M., M. Campillo, L. Stehly, and M. H. Ritzwoller (2005), High-resolution surface-wave tomography from ambient seismic noise, Science, 307, 1615–1618, doi:10.1126/ science.1108339.

Snieder, R., Gret, A., Douma, H. & Scales, J., 2002. Coda wave interfermetry for estimating nonlinear behavior in seismic velocity, Science, 295,2253–2255.

Snieder, R. (2004) Extracting the Green's function from the correlation of coda waves: A derivation based on stationary phase, Phys. Rev. E, 69, 046610

Snieder, R., K. Wapenaar, K. Larner, Spurious multiples in seismic interferometry of primaries, Geophysics, 71, SI111-SI124, 2006

Snieder, R., (2007) Extracting the Green's function of attenuating heterogeneous media from uncorrelated waves, J. Acoust. Soc. Am., 121, 2637-2643.

Spetzler, J. and R. Snieder, R., (2004) The Fresnel volume and transmitted waves, Geophysics, 69, 653-663.

Stehly, L., M. Campillo, and N. M. Shapiro (2006), A study for the seismic noise from its long-range correlation properties, J. Geophys. Res., 111, B10306, doi:10.1029/2005JB004237.

Stehly, L, M. Campillo and N. Shapiro (2007) Travel time measurements from noise correlation: stability and detection of instrumental time shifts Geophysical Journal International. doi: 10.1111/j.1365-246X.2007.03492.x

Stehly, L., M. Campillo, B. Froment and R.L. Weaver (2008) Reconstructing Green's function by correlation of the coda of the correlation (C3) of ambient seismic noise JOURNAL OF GEOPHYSICAL RESEARCH-SOLID EARTH Volume: 113 Issue: B11 Article Number: B11306 Published: NOV 21 2008

Stehly L, Fry B, Campillo M, et al. Tomography of the Alpine region from observations of seismic ambient noise GEOPHYSICAL JOURNAL INTERNATIONAL Volume: 178 Issue: 1 Pages: 338-350 2009

Stehly, L., P. Cupillard and B. Romanowicz (2011) Towards improving ambient noise tomography using simultaneously curvelet denoising filters and SEM simulation of ambient noise, C. R. Geoscience 343 (2011) 591–599

Stockwell, R. G., G. L. Mansinha and R. P. Lowe (1996), Localization of the complex spectrum: the S transform, IEEE Trans. Signal Process., 44, 998– 1001,

doi:10.1109/78.492555.

Tanimoto, T., J. Um, K. Nishida, and N. Kobayashi (1998), Earth's continuous oscillations observed on seismically quiet days, Geophys. Res. Lett., 25, 1553–1556, doi:10.1029/98GL01223.

Tibuleac, I. M. and von Seggern, D. (2012), Crust–mantle boundary reflectors in Nevada from ambient seismic noise autocorrelations. Geophysical Journal International, 189: 493–500. doi: 10.1111/j.1365-246X.2011.05336.x

Toksöz, M.N., Lacoss, R.T., 1968. Microseisms: mode structure and sources. Science 159, 872–873.

Tromp, J., Luo, Y., Hanasoge, S. & Peter, D., 2010. Noise cross-correlation sensitivity kernels, Geophys. J. Int., 183, 791–819.

Tsai, V. C. (2009). On Establishing the Accuracy of Noise Tomography Travel-Time Measurements in a Realistic Medium, Geophys. J. Int., 178, 1555-1564, doi:10.1111/j.1365-246X.2009.04239.x.

Van Vleck, J.H. and D. Middleton (1966) The spectrum of clipped noise, Proc. IEEE 54, 2-19.

Verbeke, J., Boschi, L., Stehly, L., Kissling, E. and Michelini, A. (2012), High-resolution Rayleigh-wave velocity maps of central Europe from a dense ambient-noise data set. Geophysical Journal International, 188: 1173–1187. doi: 10.1111/j.1365-246X.2011.05308.x

Vinnik, L. P. 1973 Sources of microseismic P waves. Pure Appl. Geophys. 103 (1), 282–289.

Wapenaar, K., 2004, Retrieving the elastodynamic Green's function of an arbitrary inhomogeneous medium by cross correlation: Phys. Rev. Lett., Vol. 93 (25), 254301-1 - 254301-4.

Wapenaar, K.,(2006) Nonreciprocal Green's function retrieval by cross correlation J. Acoust. Soc. Am. 120, EL7

Wapenaar, K., and J. Fokkema, 2006, Green's function representations for seismic interferometry: Geophysics, 71, no. 4, SI33–SI46, doi: 10.1190/1.2213955.

Wapenaar, K., J. van der Neut, and E. Ruigrok, "Passive seismic interferometry by multidimensional deconvolution," Geophysics 73, A51 (2008).

Wapenaar, K., D. Draganov, R. Snieder, X. Campman, and A. Verdel, Tutorial on seismic interferometry. Part 1: Basic principles and applications, Geophysics, 75, 75A195-75A209, 2010

Wapenaar, K., E. Slob, R. Snieder, and A. Curtis, Tutorial on seismic interferometry. Part 2: Underlying theory, Geophysics, 75, 75A211-75A227, 2010

Weaver, R. L. (1982). On diffuse waves in solid media, J. Acoust. Soc. Am. 71, 1608-1609.

Weaver, R.L. and Lobkis, O.I. (2001), Ultrasonics without a source: Thermal fluctuation correlation at MHz frequencies, Phys. Rev. Lett. 87, 134301–134304.

Weaver, R. L. and O. I. Lobkis (2004). Diffuse fields in open systems and the emergence of the Green's function, J. Acoust. Soc. Am. 116, 2731-2734.

Weaver R.L., Froment B, Campillo M. On the correlation of non-isotropically distributed ballistic scalar diffuse waves JOURNAL OF THE ACOUSTICAL SOCIETY OF AMERICA Volume: 126 Issue: 4 Pages: 1817-1826 2009

Weaver, RL, C. Hadziioannou, E. Larose and M. Campillo On the precision of noise correlation interferometry, Geophys. J. Int. (2011) doi: 10.1111/j.1365-246X.2011.05015.x

Wegler, U., and C. Sens-Schönfelder (2007), Fault zone monitoring with Passive Image Interferometry, Geophys. J. Int., 168, 1029–1033, doi:10.1111/j.1365-246X.2006.03284.x

Wegler, U., H. Nakahara, C. Sens-Schönfelder, M. Korn, and K. Shiomi (2009), Sudden drop of seismic velocity after the 2004 Mw 6.6 mid-Niigata earthquake, Japan, observed with Passive Image Interferometry, J. Geophys. Res., 114, B06305, doi:10.1029/2008JB005869.

Weemstra, C., L. Boschi, A. Goertz and B. Artman (2013), Seimic attenuation from recordings of ambient noise, Geophysics, 78, Q1-Q14, doi: 10.1190/GEO2012-0132.1.

Yamamoto, M., and H. Sato (2010), Multiple scattering and mode conversion revealed by an active seismic experiment at Asama volcano, Japan, J. Geophys. Res., 115, *B07304, doi:*10.1029/2009JB007109.

Yang, Y., Ritzwoller, M.H., Levshin, A.L.&Shapiro, N.M., 2007. Ambient noise Rayleigh wave tomography across Europe, Geophys. J. Int., 168, 259–274.

Yang, Y., M. H. Ritzwoller, F.-C. Lin, M. P. Moschetti, and N. M. Shapiro (2008), Structure of the crust and uppermost mantle beneath the western united states revealed by ambient noise and earthquake tomography, J. Geophys. Res., 113, B12310, doi:10.1029/2008JB005833.

Yao, H. and Van der Hilst, R.D., 2009. Analysis of ambient noise energy distribution and phase velocity bias in ambient noise tomography, with application to SE Tibet, Geophys.J. Int.,10.1111/j.1365-246X.2009.04329.x

Yao, H., R. D. van der Hilst, and M. V. de Hoop (2006), Seismic-wave array tomography in SE Tibet from ambient seismic noise and two-station analysis - I. Phase velocity maps, Geophys. J. Int., 166, 732–744, doi:10.1111/j.1365- 246X.2006.03028.x.

Yao, H., Beghein, C., and van der Hilst, R.D., 2008. Surface wave array tomography in SE Tibet from ambient seismic noise and two-station analysis: –II. Crustal and upper-mantle structure, Geophys. J. Int., 173, 205–219, doi:10.1111/j.1365-246X.2007.03696.x..

Yao, H., Gouédard, P., McGuire, J., Collins, J. and van der Hilst, R.D., 2011. Structure of young East Pacific Rise lithosphere from ambient noise correlation analysis of fundamental- and higher-mode Scholte-Rayleigh waves, Comptes Rendus Geoscience de l'Académie des Sciences, doi:10.1016/j.crte.2011.04.004

Yu, T.-C., and S.-H. Hung (2012), Temporal changes of seismic velocity associated with the 2006 Mw 6.1 Taitung earthquake in an arc-continent collision suture zone, Geophys. Res. Lett., 39, L12307, doi:10.1029/2012GL051970.

Zhan, Z., Ni, S., Helmberger,D.V.&Clayton, R.W., 2010. Retrieval of moho reflected shear wave arrivals from ambient seismic noise, Geophys. J. Int., 1, 408–420.

Zheng, S., Sun, X., Song, X., Yang, Y.&Ritzwoller, M.H., 2008. Surface wave tomography of China from ambient seismic noise correlation, Geochem. Geophys. Geosyst., 9, Q05020, doi:10.1029/2008GC001981.

Zhang, J., P. Gerstoft, and P. D. Bromirski (2010), Pelagic and coastal sources of P-wave microseisms: Generation under tropical cyclones, Geophys. Res. Lett., 37, L15301, doi:10.1029/2010GL044288.

Nom du document : Correlations_final_revised_final.doc
Répertoire : D:\boulot\michel
Modèle : C:\Documents and Settings\rouxphi\Application Data\Microsoft\Modèles\Normal.dot
Titre : Chapter Noise Correlations
Sujet :
Auteur : Michel Campillo
Mots clés :
Commentaires :
Date de création : 10/04/2013 16:51:00
N° de révision : 34
Dernier enregistr. le : 07/05/2013 17:42:00
Dernier enregistrement par : rouxphi
Temps total d'édition : 136 Minutes
Dernière impression sur : 07/05/2013 17:43:00
Tel qu'à la dernière impression
Nombre de pages : 65
Nombre de mots : 20 839 (approx.)
Nombre de caractères : 114 619 (approx.)

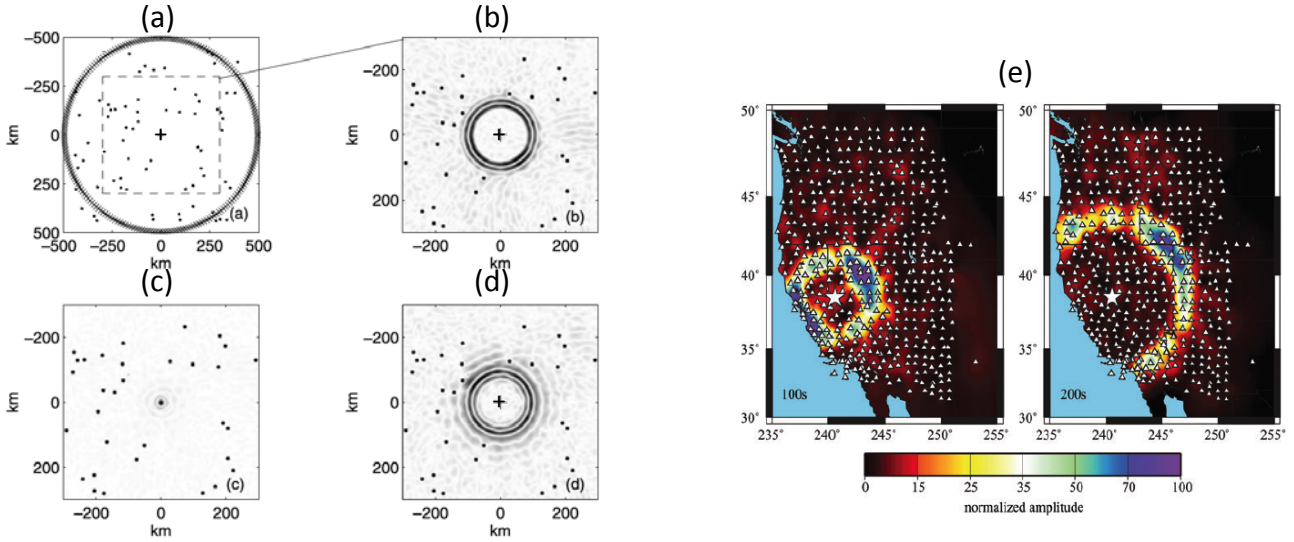
(a)
(b)
(c)
(d)
(e)
km
−500
−250
0
250
500
−200
200
100s
200s
50°
45°
40°
35°
30°
235°
240°
245°
250°
255°
0
15
25
35
50
70
100
normalized amplitude

Fig. 1

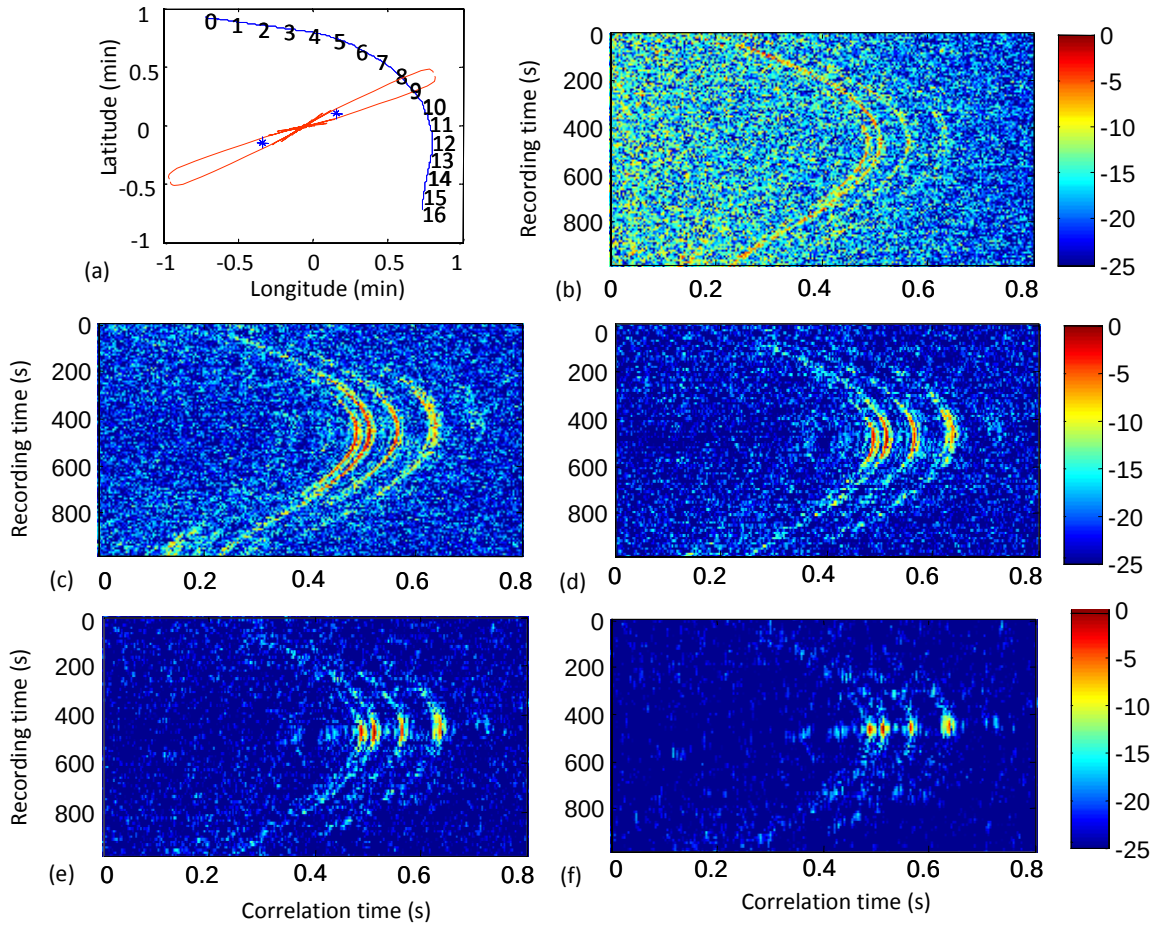
(a)
Latitude (min)
Longitude (min)
(b)
(c)
(d)
(e)
(f)
Recording time (s)
Correlation time (s)

Fig. 2

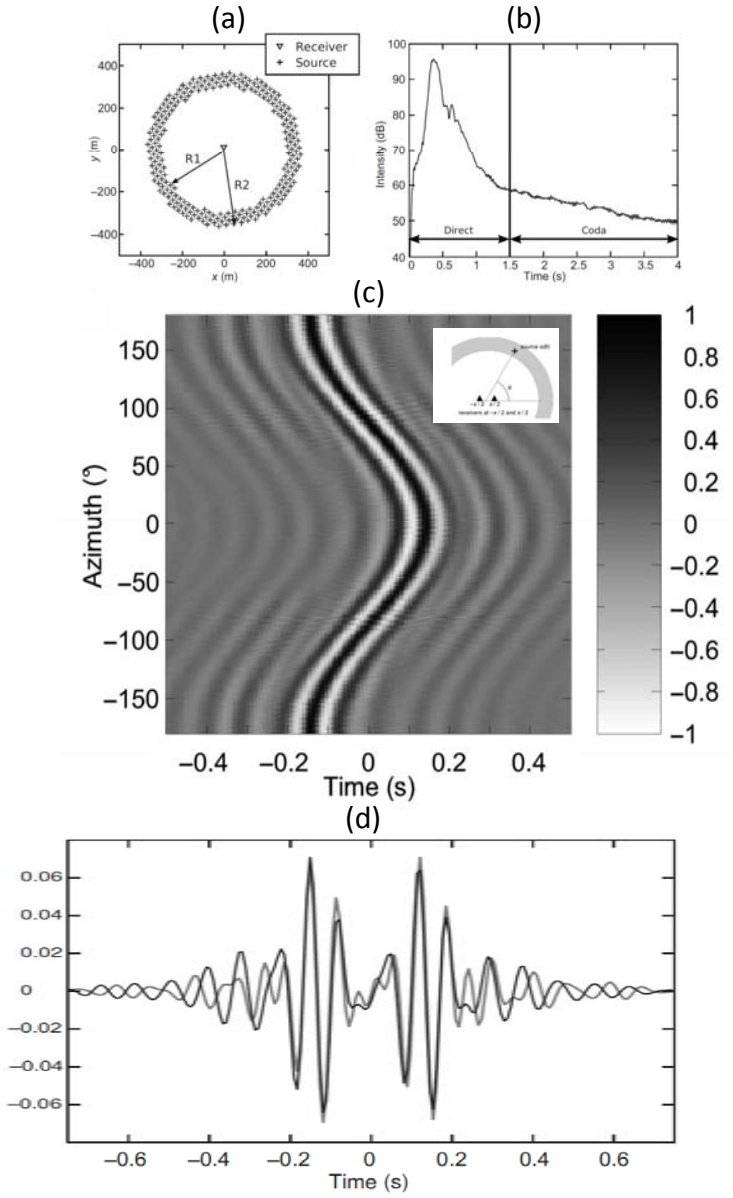
(a)
Receiver
Source
R1
R2
y (m)
x (m)
(b)
Intensity (dB)
Direct
Coda
Time (s)
(c)
Azimuth (°)
Time (s)
(d)
Time (s)

Fig. 3

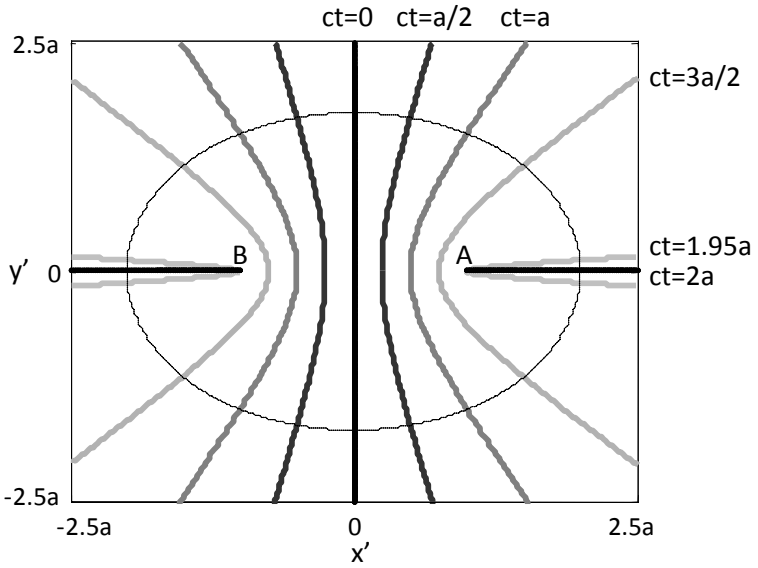

Fig. 4

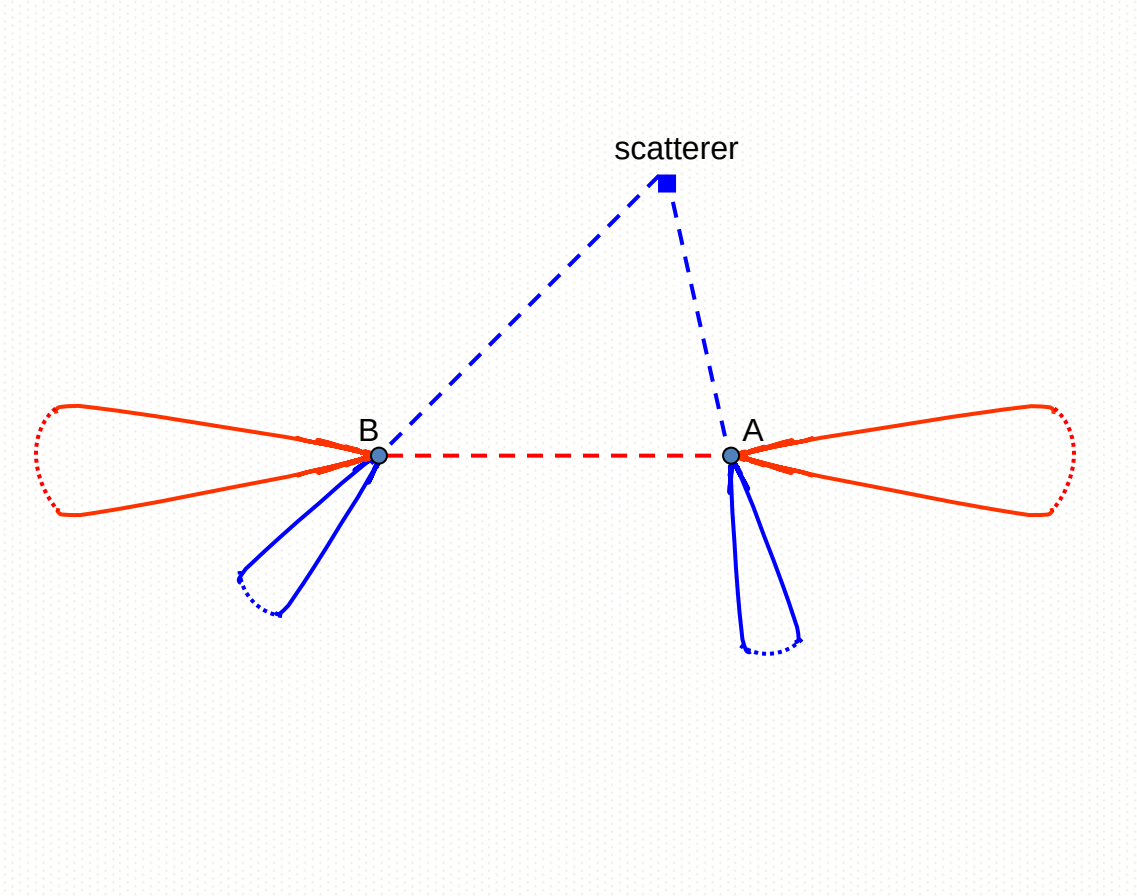

Fig. 5

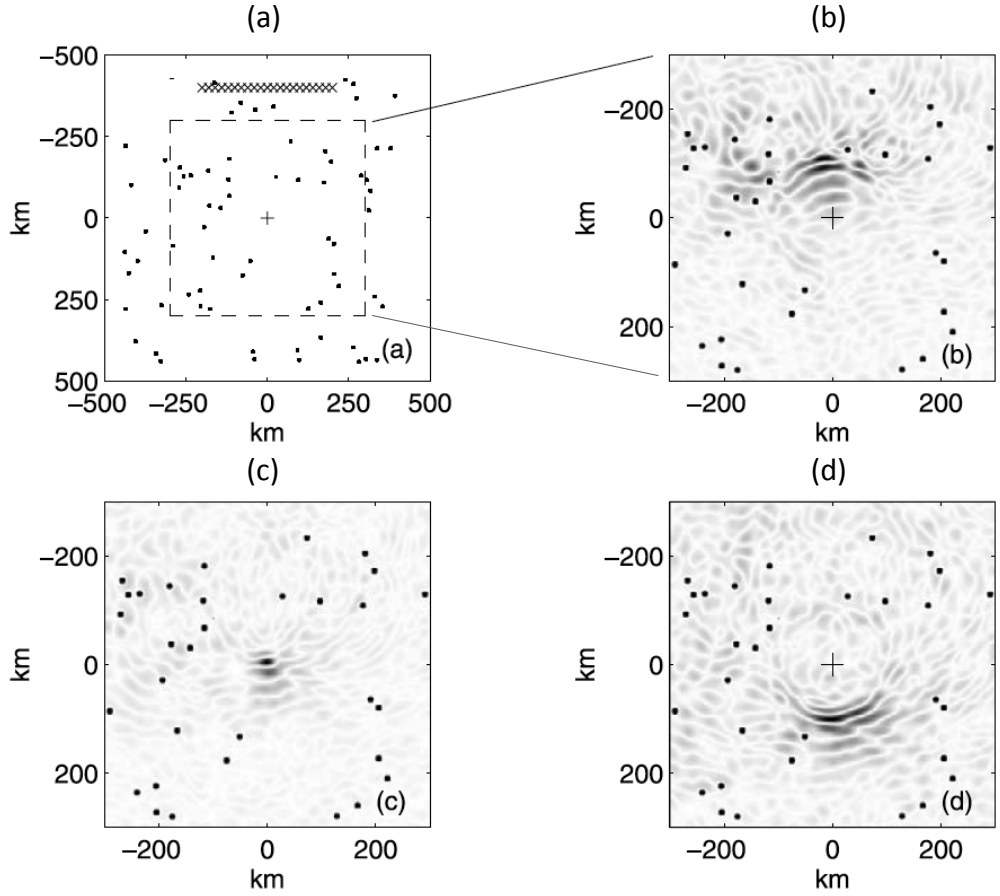

Fig. 6

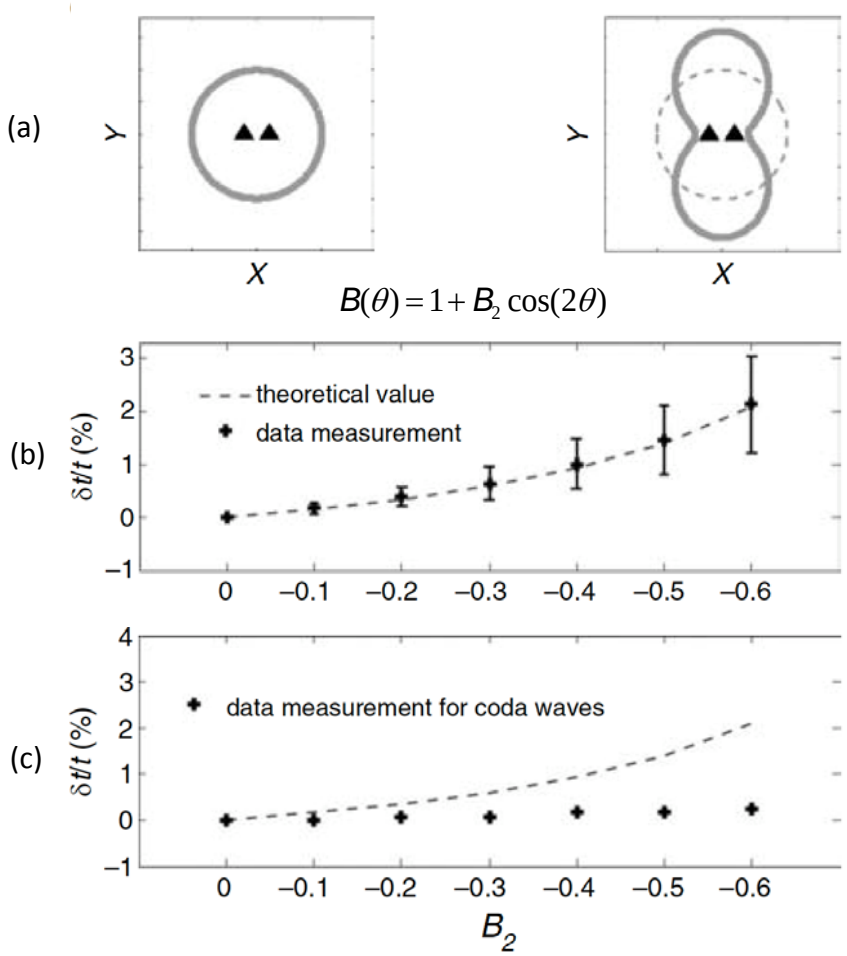
(a)
Y
X
Y
X
$B(\theta) = 1 + B_2 \cos(2\theta)$
(b)
theoretical value
data measurement
δt/t (%)
3
2
1
0
−1
0
−0.1
−0.2
−0.3
−0.4
−0.5
−0.6
(c)
data measurement for coda waves
δt/t (%)
4
3
2
1
0
−1
0
−0.1
−0.2
−0.3
−0.4
−0.5
−0.6
B_2

Fig. 7

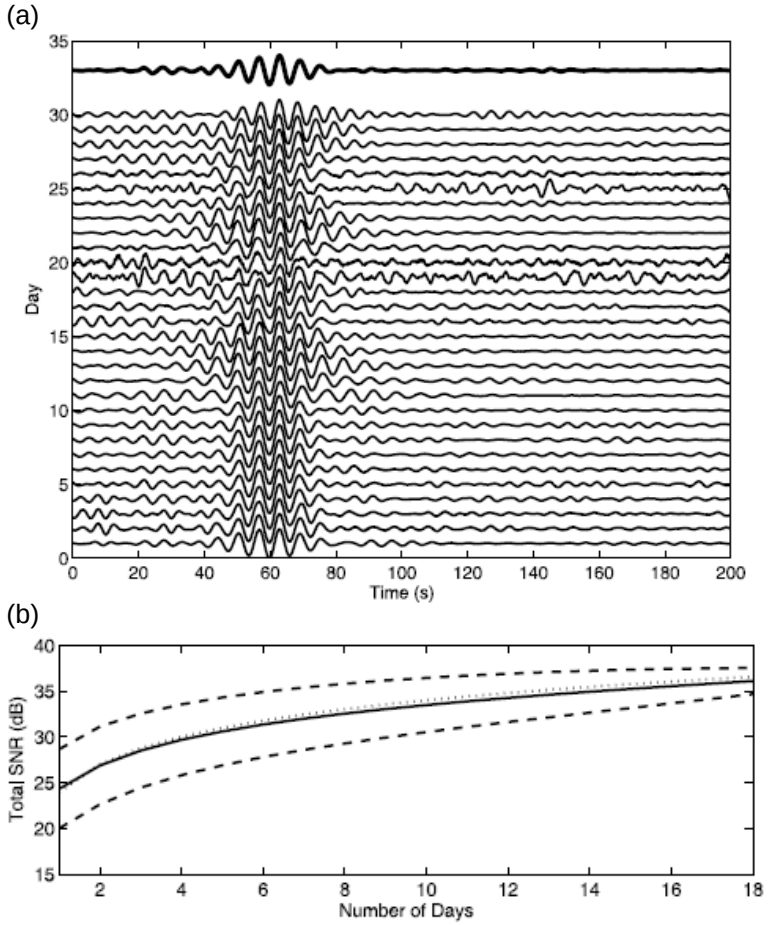

Fig. 8

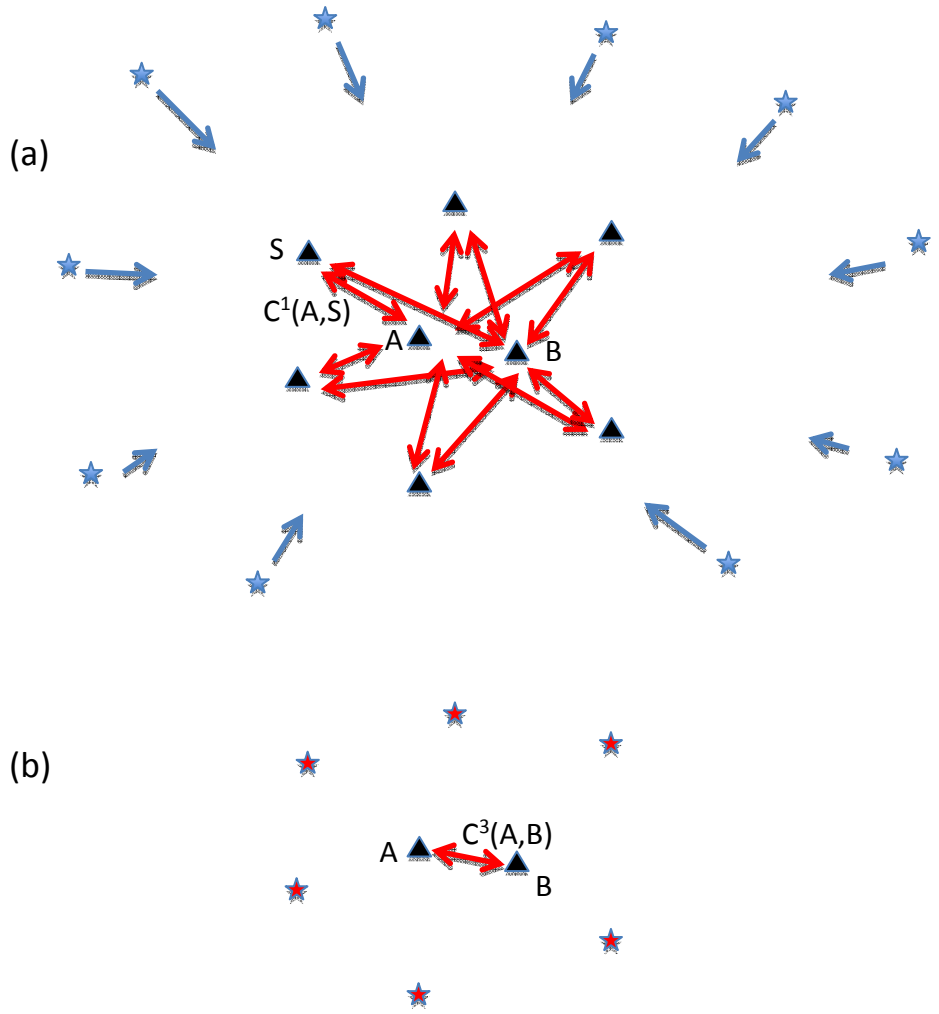

Fig. 9

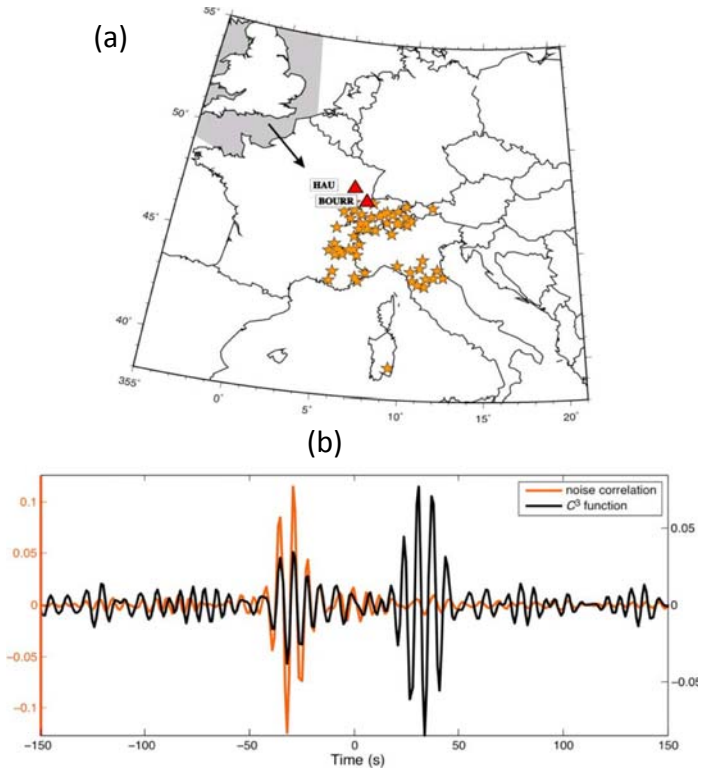
(a)
55°
50°
45°
40°
355°
0°
5°
10°
15°
20°
HAU
BOURR
(b)
noise correlation
C3 function
0.1
0.05
0
−0.05
−0.1
−150
−100
−50
0
50
100
150
Time (s)

Fig. 10

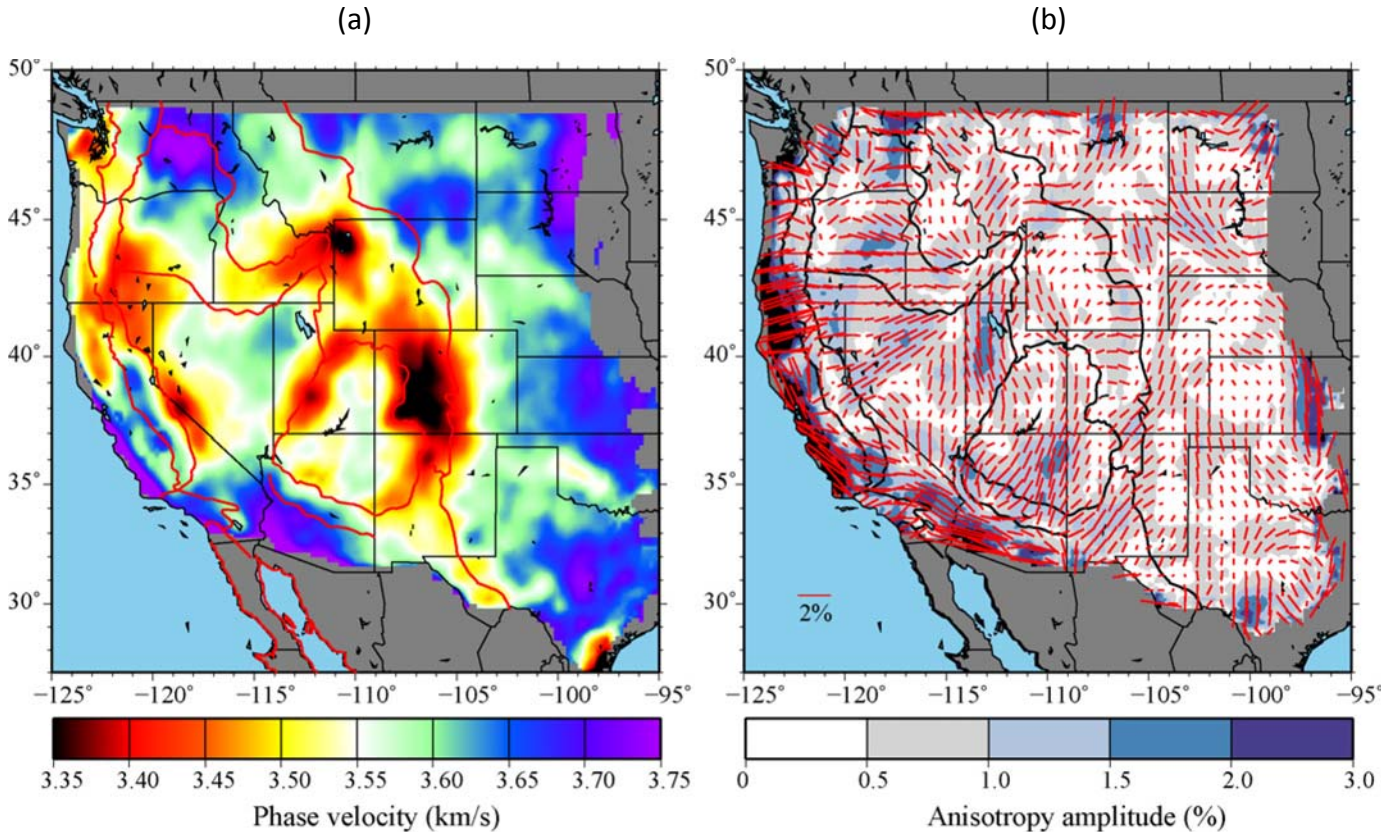
(a)
(b)
50°
45°
40°
35°
30°
−125°
−120°
−115°
−110°
−105°
−100°
−95°
3.35
3.40
3.45
3.50
3.55
3.60
3.65
3.70
3.75
Phase velocity (km/s)
2%
0
0.5
1.0
1.5
2.0
3.0
Anisotropy amplitude (%)

Fig. 11

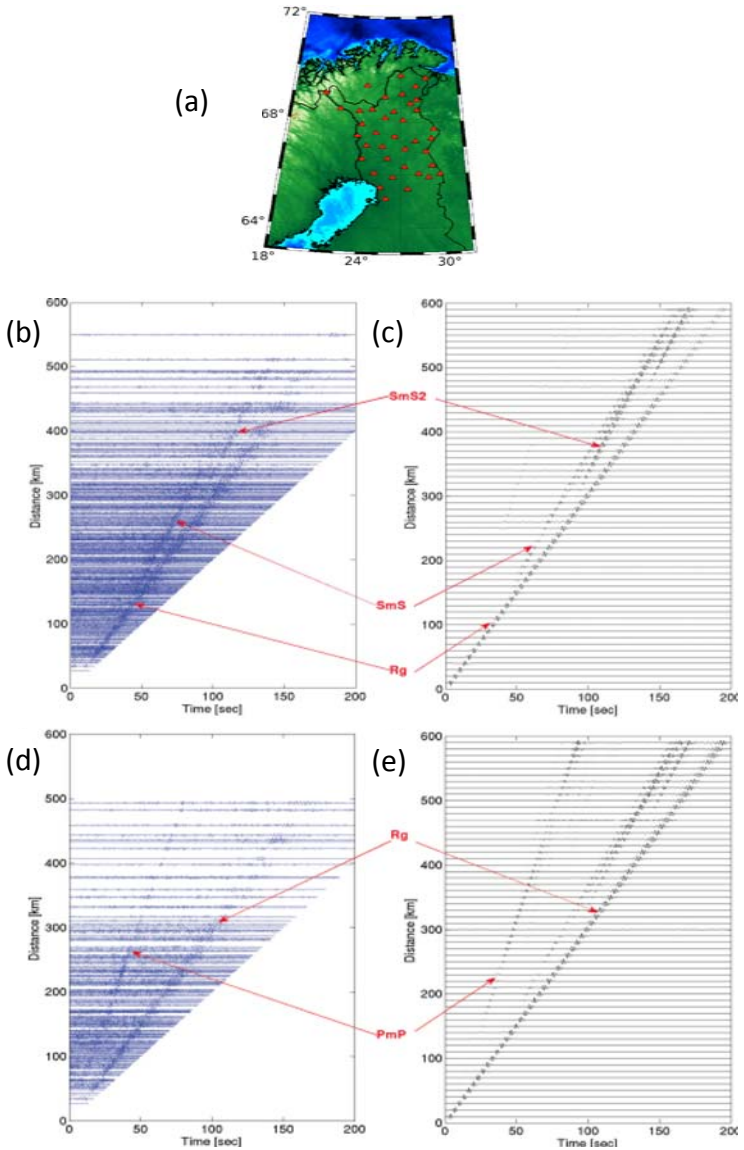

Fig. 12

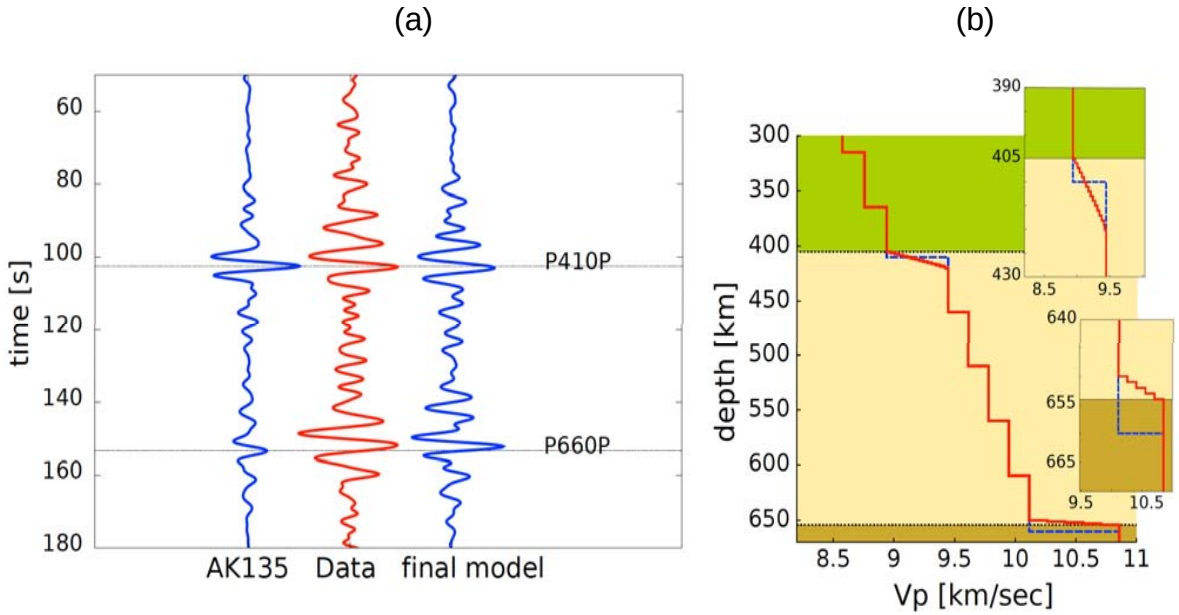
(a)
(b)
time [s]
60
80
100
120
140
160
180
P410P
P660P
AK135
Data
final model
depth [km]
300
350
400
450
500
550
600
650
390
405
430
8.5
9.5
640
655
665
9.5
10.5
8.5
9
9.5
10
10.5
11
Vp [km/sec]

Fig. 13

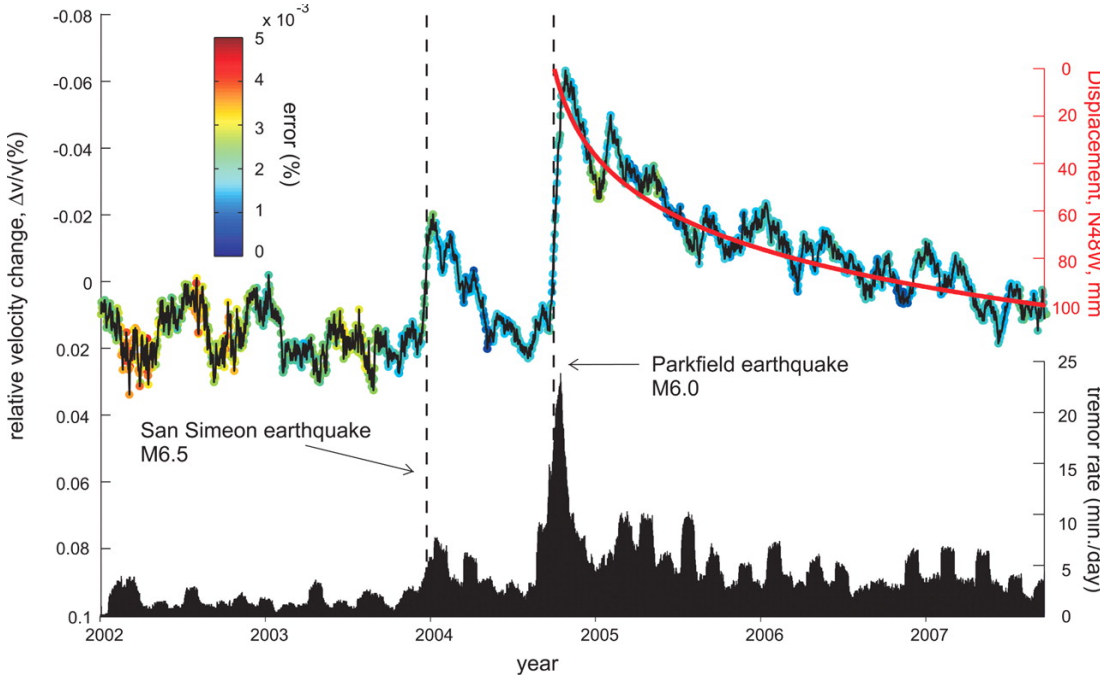
relative velocity change, Δv/v(%)
-0.08
-0.06
-0.04
-0.02
0
0.02
0.04
0.06
0.08
0.1
x 10^-3
5
4
3
2
1
0
error (%)
San Simeon earthquake
M6.5
Parkfield earthquake
M6.0
0
20
40
60
80
100
Displacement, N48W, mm
25
20
15
10
5
0
tremor rate (min./day)
2002
2003
2004
2005
2006
2007
year

Fig. 14